Numerical experiments on the interaction between the large- and small-scale motion of the Navier-Stokes Equations

By WILLIAM HENSHAW[1], HEINZ-OTTO KREISS[2] AND JACOB YSTRÖM[3]

[1]Centre for Applied Scientific Computing, Lawrence Livermore National Laboratory, Livermore, CA 94551, USA;

[2,3]Department of Mathematics, University of California at Los Angeles, Los Angeles, CA 90024, USA;

[2,3]Department of Numerical Analysis and Computing Science, Royal Institute of Technology, 10044 Stockholm, Sweden;

(Received 13 March 2002)

We consider solutions to the unforced incompressible Navier–Stokes equations in a 2π-periodic box. We split the solution into two parts representing the large-scale and small-scale motions. We define the large-scale as the sum of the first k_c Fourier modes in each direction, and the small-scale as the sum of the remaining modes. We attempt to reconstruct the small-scale by incorporating the large-scale solution as known forcing into the equations governing the evolution of the small-scale. We want to find the smallest value of k_c for which the time evolution of the large-scale sets up the dissipative structures so that the small-scale is determined to a significant degree. Existing theory based on energy estimates gives a pessimistic estimate for k_c that is inversely proportional to the smallest length-scale of the flow. At this value of k_c the energy in the small-scale is exponentially small. In contrast, numerical calculations indicate that k_c can often be chosen remarkably small. We attempt to explain why the time evolution of a relatively few number of large-scale modes can be used to reconstruct the small scale-scale modes in many situations. We also show that similar behaviour is found in solutions to Burgers' equation.

1. Introduction

The problem we want to discuss is motivated by weather prediction. Typically one divides the atmospheric motions into large-scale, mesoscale and small-scale motions. Their length scales are 1000 km, 100 km and 10 km respectively. To start a numerical weather forecast one needs initial data which must be provided by observations. Unfortunately the observational net is too sparse to obtain initial data for the meso-scale and the small-scale. This is a serious problem, since for extended forecasts one needs at least initial data for the mesoscales. Being optimistic one can argue that the observations determine the large-scale motion and due to modern measuring techniques one can observe the time history of the large-scale. If the time history of the large-scale motion determines the smaller scales, then one can think of the following process to determine the missing scales of the initial data. Assume that we want to make a weather forecast starting at time $t = 0$. To obtain the correct initial data we start at time $t = -T_0$ and assume that due to observations, we know the time history of the large-scale between $-T_0 \leq t \leq 0$. Therefore we can replace at every time step the calculated large-scale by the observed large-scale and hope that the smaller scales have adjusted to the correct values at $t = 0$.

Operational weather prediction models include many complicated physical processes including the effects of solar heating and cloud formation. It would be difficult to quantitively study the efficacy of incorporating the time history of the large-scale into this full model due to the many modeling approximations made and due to the errors made in measurements. We are thus led to study the underlying simplified models for Burgers' equation in one-dimension and the incompressible Navier–Stokes equations in two and three space dimensions.

Consider the incompressible Navier-Stokes equations for the velocity $\boldsymbol{u}$ and kinematic pressure p,

$$\boldsymbol{u}_t + (\boldsymbol{u}\cdot\boldsymbol{\nabla})\boldsymbol{u} + \boldsymbol{\nabla} p = \nu\nabla^2\boldsymbol{u}, \;\; \nu > 0, \tag{1.1a}$$

$$\boldsymbol{\nabla}\cdot\boldsymbol{u} = 0, \tag{1.1b}$$

with initial conditions given at time t_0

$$\boldsymbol{u}(\boldsymbol{x}, t_0) = \boldsymbol{u}_0(\boldsymbol{x}), \tag{1.1c}$$

and with periodic boundary conditions on the box with sides of length 2π and volume $\mathcal{V}$. For every fixed $t \geq t_0$ we can expand the solution into a Fourier series

$$\boldsymbol{u}(\boldsymbol{x}, t) = \sum_{\boldsymbol{k}} \hat{\boldsymbol{u}}(\boldsymbol{k}, t) e^{i\boldsymbol{k}\cdot\boldsymbol{x}}, \;\; p(\boldsymbol{x}, t) = \sum_{\boldsymbol{k}} \hat{p}(\boldsymbol{k}, t) e^{i\boldsymbol{k}\cdot\boldsymbol{x}}. \tag{1.2}$$

Here $\boldsymbol{k} = (k_1, k_2, k_3)^T$ is a multi-index with $k = |\boldsymbol{k}| = \sqrt{k_1^2 + k_2^2 + k_3^2}$. Let k_c be a natural number representing the wave-number at which we divide the solution into the large and small scales. We split $\boldsymbol{u}$ into two parts, $\boldsymbol{u} = \boldsymbol{u}^I + \boldsymbol{u}^{II}$ where

$$\boldsymbol{u}^I(\boldsymbol{x}, t) = \mathcal{P}^I\boldsymbol{u} := \sum_{|\boldsymbol{k}| \leq k_c + 1/2} \hat{\boldsymbol{u}}(\boldsymbol{k}, t) e^{i\boldsymbol{k}\cdot\boldsymbol{x}},$$

$$\boldsymbol{u}^{II}(\boldsymbol{x}, t) = \mathcal{P}^{II}\boldsymbol{u} := \sum_{|\boldsymbol{k}| > k_c + 1/2} \hat{\boldsymbol{u}}(\boldsymbol{k}, t) e^{i\boldsymbol{k}\cdot\boldsymbol{x}}.$$

We call $\boldsymbol{u}^I = \mathcal{P}^I\boldsymbol{u}$ the large-scale and $\boldsymbol{u}^{II} = \mathcal{P}^{II}\boldsymbol{u}$ the small-scale. The operators $\mathcal{P}^I$ and $\mathcal{P}^{II}$ are projections with $\mathcal{P}^I + \mathcal{P}^{II} = I$. Let

$$\|\boldsymbol{u}\|^2 = \|\boldsymbol{u}(\cdot, t)\|^2 = \int_{\mathcal{V}} |\boldsymbol{u}(\boldsymbol{x}, t)|^2 \, \mathrm{d}\boldsymbol{x},$$

denote the usual L_2 norm. The kinetic energy per unit mass and enstrophy per unit mass are denoted by

$$E_K = E_K(\boldsymbol{u}) = \frac{1}{2\mathcal{V}}\|\boldsymbol{u}\|^2, \;\; \Omega = \Omega(\boldsymbol{u}) = \frac{1}{2\mathcal{V}}\|\boldsymbol{\xi}\|^2,$$

respectively and where $\boldsymbol{\xi} = \boldsymbol{\nabla}\times\boldsymbol{u}$ is the vorticity.

In three-dimensions we will choose the wave-number k_c in such a way that the kinetic energy of the large-scale is large compared to the kinetic energy of the small scale. In many turbulent flows most of the kinetic energy is contained in the long waves and k_c can be chosen rather small independently of the viscosity ν.

We can write the Navier–Stokes equations as a system for the large-scale and the small-scale respectively,

$$\boldsymbol{u}^I_t + \mathcal{P}^I\left[((\boldsymbol{u}^I + \boldsymbol{u}^{II})\cdot\boldsymbol{\nabla})\boldsymbol{u}^I + (\boldsymbol{u}^I\cdot\boldsymbol{\nabla})\boldsymbol{u}^{II}\right] + \boldsymbol{\nabla} p^I = \nu\nabla^2\boldsymbol{u}^I + \boldsymbol{F}^I(\boldsymbol{u}^{II}), \tag{1.3a}$$

$$\boldsymbol{\nabla}\cdot\boldsymbol{u}^I = 0, \tag{1.3b}$$

$$\boldsymbol{u}^{II}_t + \mathcal{P}^{II}\left[((\boldsymbol{u}^I + \boldsymbol{u}^{II})\cdot\boldsymbol{\nabla})\boldsymbol{u}^{II} + (\boldsymbol{u}^{II}\cdot\boldsymbol{\nabla})\boldsymbol{u}^I\right] + \boldsymbol{\nabla} p^{II} = \nu\nabla^2\boldsymbol{u}^{II} + \boldsymbol{F}^{II}(\boldsymbol{u}^I), \tag{1.4a}$$

$$\boldsymbol{\nabla}\cdot\boldsymbol{u}^{II}=0, \tag{1.4b}$$

where

$$\boldsymbol{F}^{I}(\boldsymbol{u}^{II})=-\mathcal{P}^{I}\left[(\boldsymbol{u}^{II}\cdot\boldsymbol{\nabla})\boldsymbol{u}^{II}\right],\quad \boldsymbol{F}^{II}(\boldsymbol{u}^{I})=-\mathcal{P}^{II}\left[(\boldsymbol{u}^{I}\cdot\boldsymbol{\nabla})\boldsymbol{u}^{I}\right].$$

Assume to begin with that we know the initial data

$$\boldsymbol{u}^{II}(\boldsymbol{x},t_0)=\boldsymbol{u}_0^{II}(\boldsymbol{x}), \tag{1.5}$$

of the small-scale and the time evolution of the large-scale, that is we know $\boldsymbol{u}^{I}(\boldsymbol{x},t),\ t\geq t_0$. Then we can use (1.4) and (1.5) to exactly reconstruct the small-scale. Now assume that we do not know the initial data for the small-scale but do know $\boldsymbol{u}^{I}$ as a function of space and time. If we solve (1.4) with zero initial data then we will generate a new approximate solution that we call the *playback* solution, $\{\boldsymbol{u}_p,p_p\}=\{\boldsymbol{u}_p^{I}+\boldsymbol{u}_p^{II},p_p^{I}+p_p^{II}\}$ satisfying $\{\boldsymbol{u}_p^{I},p_p^{I}\}=\{\boldsymbol{u}^{I},p^{I}\}$ and

$$\partial_t\boldsymbol{u}_p^{II}+\mathcal{P}^{II}\left[((\boldsymbol{u}^{I}+\boldsymbol{u}_p^{II})\cdot\boldsymbol{\nabla})\boldsymbol{u}_p+(\boldsymbol{u}_p^{II}\cdot\boldsymbol{\nabla})\boldsymbol{u}^{I}\right]+\boldsymbol{\nabla}p_p^{II}=\nu\nabla^2\boldsymbol{u}_p^{II}+\boldsymbol{F}^{II}(\boldsymbol{u}^{I}), \tag{1.6a}$$

$$\boldsymbol{\nabla}\cdot\boldsymbol{u}_p^{II}=0, \tag{1.6b}$$

$$\boldsymbol{u}_p^{II}(\boldsymbol{x},t_0)=0. \tag{1.6c}$$

The question we want to answer is how large must we choose k_c so that the small-scale is recovered at some future time T. Define the relative error in the small-scale by

$$e_p(t)=\frac{\|\boldsymbol{u}_p^{II}(\cdot,t)-\boldsymbol{u}^{II}(\cdot,t)\|^2}{\|\boldsymbol{u}^{II}(\cdot,t)\|^2}. \tag{1.7}$$

DEFINITION 1. *We say that the* **large-scale determines the small-scale**, *to an accuracy of* ϵ, *at some future time* $T=O(1)$, *if the relative error at* T *is less than* ϵ,

$$e_p(T)<\epsilon.$$

Note that we consider the initial value problem with no external forcing and thus

$$\lim_{t\to\infty}\|\boldsymbol{u}(\cdot,t)\|=0.$$

Our results are only of interest if the small scale is recovered at a time T before the solution has decayed to a point where it behaves essentially as a solution to the heat equation. If the equation for the small-scale were linear and uncoupled to the large-scale then it would not be possible for the large-scale to determine the small-scale. The coupling of the large-scale and small-scale through the nonlinear terms is thus critical.

In section 2 we first examine solutions to Burgers' equation to see when the small-scale can be reconstructed from the time history of the large-scale. The results show that even for very small values of k_c the small-scale features associated with the large-scale shocks are quickly recovered. We argue that the large-scale acts to create the dissipative structures (shocks) and that errors in the playback solution are propagated into the shocks along characteristics where they are converted to high-frequencies that can be effectively damped by viscous dissipation. Although in general the large-scale appears to determine much of the small-scale there can of course be small-scale features that are not strongly coupled to the large-scale and thus will not be reconstructed.

In section 3 we consider the Navier-Stokes equations. We give some heuristic arguments to suggest when the time history of the large-scale might determine the small-scale. In sections 4 and 5 we present numerical results for two-dimensional and three-dimensional Navier–Stokes equations, respectively. These results show fairly generic cases when the large-scale does determine the small-scale provided the large-scale contains a significant fraction of the enstrophy in two-dimensions or energy in three-dimensions.

The approach we discuss here is related to the process of *continuous data assimilation* (or *four dimensional data assimilation*) in meteorology, originally advocated by Charney *et al.* (1969) and Thompson (1969). See Daley (1991), chapter 12, for a nice overview. Our computations here are in the spirit of the so called *identical twin experiment* which avoids the problems with uncertainties in the model by generating synthetic data directly from the model itself, rather than using measurements, see for example Williamson & Dickinson (1972) and Talagrand (1981). Typically this approach assumes that time dependent data is available for only some of the variables (such as the temperature which can be measured by satelite) and then asks when the remaining variables can be recovered. Analysis of the approach is often for a linearized model such as the shallow water equations. The effects of nonlinearity are often characterized as making the problem harder. In contrast our results show how the nonlinearities can sometimes give improved results.

In other related work Chorin *et al.* (1999) study how to predict the solution to time dependent PDEs with under-resolved computations but when prior statistical properties of the solutions are known.

2. Burgers equation

Burgers' equation is a well known model for analysing properties of shocks and turbulence, see for example Lesiuer (1990), Tatsumi (1980), and Whitham (1974). It is a simple equation that combines nonlinear wave propagation with diffusion. It models more complicated systems in situations where these two processes are the dominant effects. We consider the solution of Burgers' equation

$$u_t + uu_x = \nu u_{xx}, \tag{2.1a}$$

on the interval $[0, 2\pi]$ with initial conditions

$$u(x, 0) = f(x). \tag{2.1b}$$

We are interested in real solutions which are 2π-periodic in x and we assume that the initial conditions are reasonably smooth. Although the exact solution to Burgers' equation can be determined from the Cole-Hopf transformation, see for example Whitham (1974), we will only use arguments based on energy estimates and the method of characteristics.

We shall give a proof based on energy estimates to show that some number of large-scale modes of Burgers' equation determine the small-scale modes. The idea of the proof is due to Constantin, Foias & Temam (1984) and variants of it have been used by several authors, for example Foias & Temam (1984); Constantin, Foias, Manley & Temam (1985); Foias & Titi (1984); Jones & Titi (1993); Constantin, Doering & Titi (1996). Unfortunately the energy estimates predict that the number of large-scale modes needed is of the order $k_c = O(|f|_\infty/\nu)$. In this case the remaining small scale modes are exponentially small,

$$\sum_{|k|\geq k_c+1/2} |\hat{u}(k,t)|^2 \leq K\mathrm{e}^{-\delta k_c},$$

where K and $\delta > 0$ are some constants. From our numerical computations we know that this estimate for k_c is, in general, much too pessimistic; we shall present some arguments so show why k_c can often be chosen much smaller (perhaps independently of ν).

We will see below that question of whether the large-scale determines the small-scale is related to the question of whether perturbations in the small-scale are rapidly damped. For intermediate small scale modes with wave-number k where $k_c < k \ll \nu^{-1/2}$ the diffusion term will have little effect in damping perturbations over an $O(1)$ time interval. However, due to its nonlinear nature, Burgers' equation sets up dissipative structures that are effective at damping these intermedi-

ate wave numbers. We will argue that the large-scale modes set up the shocks (the dissipative structures) and also convect perturbations into the shock regions where they are compressed and dissipated by viscosity.

We proceed by decomposing the solution into the low and high frequency Fourier modes, $u = u^I + u^{II}$. We consider the situation when the large-scale $u^I(x,t)$ is known for $t \geq 0$. Let $\mathcal{P}^{II}$ denote the operator that projects a function onto the small-scale,

$$u^{II} = \mathcal{P}^{II} u.$$

By substituting $u = u^I + u^{II}$ into (2.1*a*,2.1*b*) and applying the projection $\mathcal{P}^{II}$ to the result we obtain an equation for the small-scale u^{II} as a function of the large-scale u^I,

$$u^{II}_t + \mathcal{P}^{II}[u^I u^{II}_x + u^I_x u^{II} + u^{II} u^{II}_x] = \nu u^{II}_{xx} + \mathcal{P}^{II} F(u^I), \tag{2.2a}$$

with initial conditions

$$u^{II}(x,0) = f^{II}(x), \tag{2.2b}$$

and where $F(u^I)$ is defined by

$$F(u^I) = -u^I_t - u^I u^I_x + \nu u^I_{xx}. \tag{2.2c}$$

We compare the solution of (2.2) with the solution to the same equations but with zero initial conditions, (in other words we perturb the initial conditions in the small-scale modes by setting them to zero),

$$\partial_t u^{II}_p + \mathcal{P}^{II}[u^I \partial_x u^{II}_p + \partial_x u^I u^{II}_p + u^{II}_p \partial_x u^{II}_p] = \nu \partial^2_x u^{II}_p + \mathcal{P}^{II} F(u^I), \tag{2.3a}$$

with initial conditions

$$u^{II}_p(x,0) = 0. \tag{2.3b}$$

We call $u_p = u^I + u^{II}_p$ the *playback solution* and are interested in knowing whether u^{II}_p converges to u^{II} by some time T, where $T = O(1)$. Note that since the solution converges to zero at $t \to \infty$, $u^{II} - u^{II}_p$ will go to zero eventually. We are not, however, interested in this long time behaviour. The error in the small-scale, $w = u^{II} - u^{II}_p$, satisfies

$$w_t + \mathcal{P}^{II}[u^I w_x + u^I_x w + \frac{1}{2}((u^{II} + u^{II}_p)w)_x] = \nu w_{xx}, \tag{2.4a}$$

obtained by subtracting (2.3a) from (2.2a). This equation can also be written as

$$w_t + \mathcal{P}^{II}[(uw)_x - \frac{1}{2}(w^2)_x] = \nu w_{xx}. \tag{2.4b}$$

The initial conditions for w are

$$w(x,0) = f^{II}(x) = u^{II}(x,0). \tag{2.4c}$$

We are interested in showing that there exists a time $T = O(1)$ when the relative error in the playback solution becomes small. We define the relative error in the playback solution as

$$e_p(t) = \frac{\|u^{II}(\cdot,t) - u^{II}_p(\cdot,t)\|^2}{\|u^{II}(\cdot,t)\|^2} = \frac{\|w(\cdot,t)\|^2}{\|u^{II}(\cdot,t)\|^2}.$$

We divide by the energy in the small-scale of the reference solution to account for the overall decay of the solution.

We first show that by choosing k_c sufficiently large the absolute error will decay exponentially fast to zero.

PROPOSITION 1. *The error in the playback solution, $\boldsymbol{u}_p$ will go to zero provided we choose*

the cut-off wavenumber k_c according to

$$k_c > \sqrt{\frac{\alpha + \overline{|u_x|}_\infty}{2\nu}}.$$

for any $\alpha > 0$. In particular we have the result that

$$\|w\| \leq \mathrm{e}^{-\alpha(t-t_0)}\|u^{II}(\cdot,t_0)\|.$$

Here

$$\overline{|u_x|}_\infty = \sup_{t\geq t_0} |u_x(\cdot,t)|_\infty \ .$$

The time $t_0 \geq 0$ has been introduced since $|u_x(\cdot,0)|_\infty$ could be infinite.

Proof:

Taking the inner product of w with (2.4*b*) gives,

$$(w,w_t) + (w,\mathcal{P}^{II}[(uw)_x - \frac{1}{2}(w^2)_x]) = \nu(w,w_{xx}) \tag{2.5}$$

In order to use integration by parts to simplify this expression we need to treat the second term which contains the operator $\mathcal{P}^{II}$. Using Parseval's equation it follows that $\mathcal{P}^{II}$ is a self-adjoint operator since for any two sufficiently smooth functions f and g

$$(f,\mathcal{P}^{II}g) = 2\pi \sum_{|k|>k_c} \hat{f}_k^* \hat{g}_k = (\mathcal{P}^{II}f, g).$$

Now since $w = \mathcal{P}^{II}w$ it follows that

$$(w,\mathcal{P}^{II}[(uw)_x - \frac{1}{2}(w^2)_x]) = (\mathcal{P}^{II}w,[(uw)_x - \frac{1}{2}(w^2)_x]) = (w,[(uw)_x - \frac{1}{2}(w^2)_x]).$$

Whence equation (2.5) can be written without the projection

$$(w,w_t) + (w,(uw)_x - \frac{1}{2}(w^2)_x) = \nu(w,w_{xx}).$$

Integration by parts gives

$$\frac{1}{2}\frac{\partial}{\partial t}\|w\|^2 = -\frac{1}{2}(w,u_x w) - \nu\|w_x\|^2. \tag{2.6}$$

where we have used $(w,(w^2)_x) = 0$ and $(w,(uw)_x) = \frac{1}{2}(w,u_x w)$. Equation (2.6) indicates how the energy in the error decays over time.

The first term on the right-hand-side can be estimated, for $t \geq t_0$, with the bound $|(w,u_x w)| \leq |u_x|_\infty \|w\|^2$. Since the first k_c Fourier modes of w are zero it follows that $\|w_x\|^2 > k_c^2\|w\|^2$. Therefore

$$\frac{1}{2}\frac{\partial}{\partial t}\|w\|^2 \leq (\frac{1}{2}|u_x|_\infty - \nu k_c^2)\|w\|^2.$$

If we choose

$$k_c > \sqrt{\frac{\alpha + \overline{|u_x|}_\infty}{2\nu}}. \tag{2.7}$$

then

$$\frac{1}{2}\frac{\partial}{\partial t}\|w\|^2 \leq -\alpha\|w\|^2$$

for $t \geq t_0$ and therefore $\|w(\cdot,t)\|$ will decay exponentially fast to zero,

$$\|w(\cdot,t)\| \leq \exp(-\alpha(t-t_0))\|w(\cdot,t_0)\|.$$

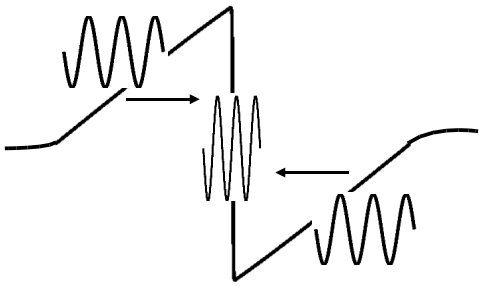

FIGURE 1. This figure illustrates a conjectured mechanism for the partial removal of errors in the playback solution for Burgers' equation. Errors in smooth regions of the flow are advected to the shock where they are compressed and damped by the viscous dissipation. The nonlinear coupling between the large- and small-scale motion can thus increase the effective dissipation of the error.

This completes the proof □

Unfortunately the bound (2.7) is quite pessimistic and is a result of using the crude estimates for the terms on the right-hand-side of equation (2.6). To see how bad this bound is we can estimate the size of $|u_x|_\infty$ as follows. Consider a solution to Burgers' equation with a shock where the solution varies from the state u_L on the left to the state u_R on the right. We define the shock strength to be the positive number $S = u_R - u_L$. Dimensional analysis shows that the width of the viscous shock profile is order ν/S and thus

$$|u_x|_\infty \leq K\frac{S^2}{\nu}, \tag{2.8}$$

for some constant K. Therefore, from (2.8) and (2.7), we obtain the estimate that the cut-off wave number should be at least $k_c = O(S/\nu)$ in order that the large-scale determine the small-scale. Numerical results strongly suggest that this estimate is usually much too large.

We shall now outline some arguments that suggest why in practice we can often choose k_c to be much smaller than $O(S/\nu)$.

2.1. *Burgers' equation with a single shock*

We first consider a specific example of reconstructing the small-scale for a single periodic sawtooth shock. Figure (2) shows the solution to Burgers' equation on the interval $\Omega = [-1, 1]$ for initial conditions equal to a sine wave. Starting at time $t = .5$ when the shock has formed we then compute the playback solution by our reconstruction procedure. The errors in the playback solution are shown in figures (2-3). See the discussion in section (2.3) for further details.

The full solution can be approximated by sawtooth shock which is of the form

$$u(x,t) \approx \begin{cases} M(t)\,(x+1) & \text{for } -1 \leq x < -b \\ M(t)\,(x-1) & \text{for } b < x < 1 \end{cases} \tag{2.9}$$

Here $M = S/2 > 0$ and $b = O(\nu/M) \ll 1$ is the approximate width of the shock. From figure (2) it can be seen that the error in the small scale, w, at time $t = 3$ is smooth away from the shock. At the shock there is a sharp layer where w transitions from its maximum value to minimum value. An examination of the error over time indicates that w is always smooth away from the shock and usually has a sharp layer at $x = 0$. It appears that the shock region acts as a sink for the errors which are advected into the shock and dissipated.

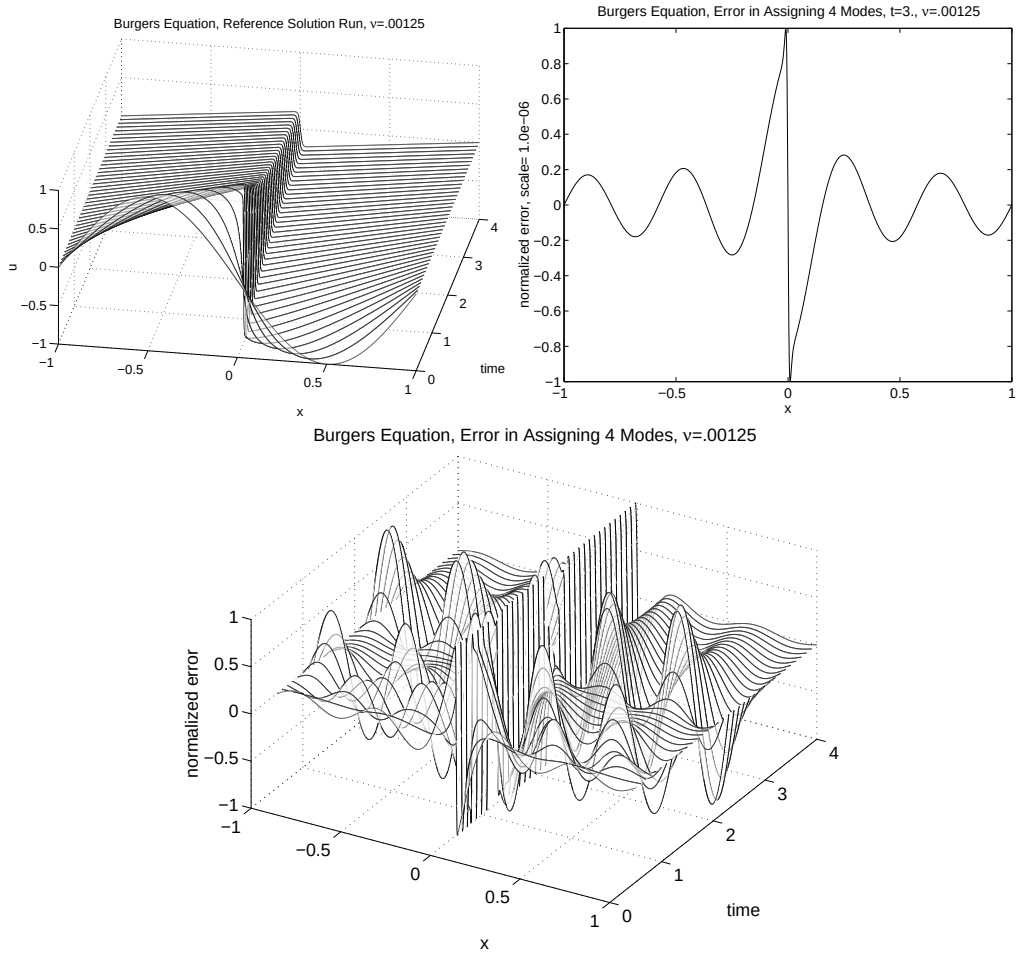

FIGURE 2. Burgers' equation: on the top left is the solution over time for an initial condition consisting of a sine wave. On the top right is the error in the playback solution at $t = 3$ when assigning $k_c = 4$ modes. On the bottom is the normalized error over time for $k_c = 4$; the error is normalized to have a maximum of 1 at each fixed time. The error is smooth away from the shock and usually largest near the shock.

Consider the energy estimate for the error, equation (2.6),

$$\begin{aligned}\frac{1}{2}\frac{\partial}{\partial t}\|w\|^2 &= -\frac{1}{2}(w, u_x w) - \nu\|w_x\|^2 \\ &\equiv \mathcal{I}(w,u).\end{aligned}$$

We wish to show that the right hand side to this expression will be less than zero. Split the interval $\Omega = [-1,1]$ into the region $B = [-b,b]$ near the shock where $u_x \le 0$ and the region $\Omega - B$ where $u_x \ge 0$. Here $b = O(\nu/M)$ is the point near the shock where u reaches a maximum and $u_x(\pm b, t) = 0$. The integral $\mathcal{I}$ can be split into two pieces

$$\begin{aligned}\mathcal{I}(w,u) &= \int_{\Omega-B} -\frac{1}{2}u_x w^2 - \nu w_x^2 \, dx + \int_{-b}^{b} -\frac{1}{2}u_x w^2 - \nu w_x^2 \, dx \\ &= I(w,u) + I_b(w,u)\end{aligned}$$

Using the approximate form given by the sawtooth shows that the integral outside the shock

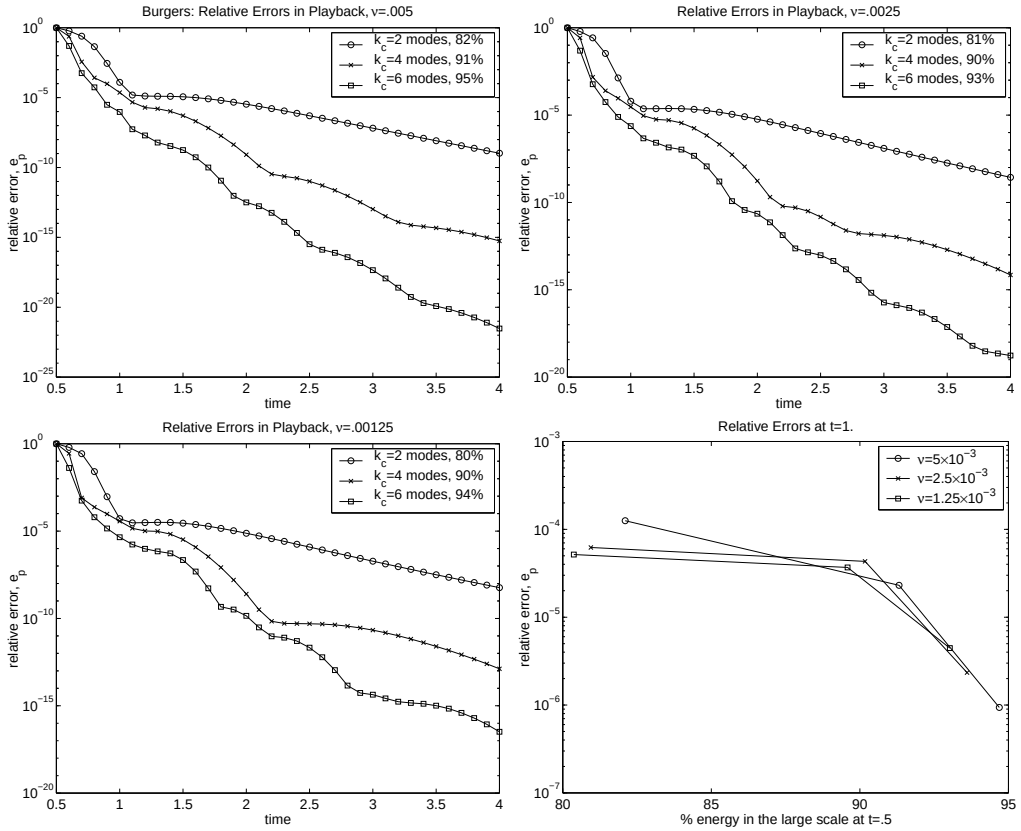

FIGURE 3. Burgers' equation with initial conditions equal to a sine wave: the relative errors, $e_p(t) = \|w\|^2/\|u^{II}\|^2$, in the high modes for the playback solutions. The lowest k_c modes of the playback solution are kept equal to those of the reference solution. The higher modes, $k > k_c$, are computed by solving Burgers' equation but with zero initial conditions. As time evolves the higher modes are recovered. The relative error decreases rapidly even for relatively small values of k_c. The caption shows the value of k_c for each curve and the percentage of energy contained in the large scale at $t = .5$.

region is negative

$$I(w,u) \approx -\int_{\Omega - B} \frac{1}{2} M w^2 + \nu w_x^2 \, dx \; .$$

It is more difficult to estimate the integral $I_b(w,u)$ since $u_x \leq 0$. We can obtain an approximate form for u valid in B as follows. Integrating Burgers' equation from $-b$ to a point x gives

$$\nu u_x = \frac{1}{2}(u^2 - M^2) + \int_{-b}^{x} u_t \, dx$$

where we have used $u_x(-b,t) = 0$ and $u(-b,t) = M(t)$. If we assume that the shock profile for u is quasi-stationary then $u_t = O(1)$ and $\int_{-b}^{x} u_t \, dx = O(b) \ll 1$. Whence, to leading order, the approximation $\tilde{u}$ to u is given by the solution to

$$\nu \tilde{u}_x = \frac{1}{2}(\tilde{u}^2 - M^2) \; .$$

This equation can be solved to give the approximate form of u through the shock

$$\tilde{u} = -M \tanh(\frac{Mx}{2\nu}) \; . \tag{2.10}$$

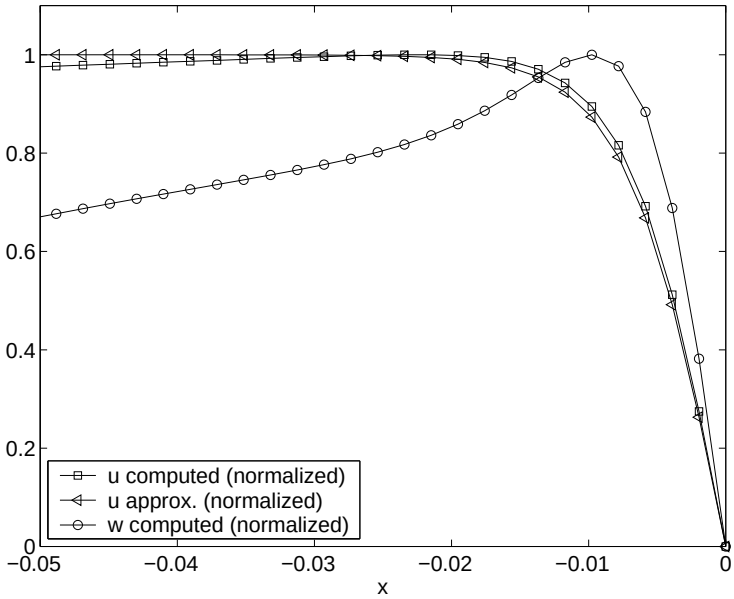

FIGURE 4. Burgers' equation: A comparison in the shock region of the computed solution for u to the approximate solution $\bar{u} = -M\tanh(Mx/(2\nu))$ for $\nu = .00125$. The error w is also shown for $k_c = 4$, $t = 3.$. The functions are normalized to have a maximum value of 1.

Figure (4) compares this approximation to the actual solution and also shows the typical form of w within the shock region.

Consider now the integral I_b. Since u_x, w^2 and w_x^2 are even functions we can also write

$$I_b(w) = -2\int_0^b \frac{1}{2}u_x w^2 + \nu w_x^2\, dx.$$

To obtain an upper bound for I_b we use a variational argument. We set $w(b) = w_1$ and determine the function, $\bar{w}$, that maximizes $I_b(\omega)$ over all functions $w \in C^2$ with boundary data $w(0) = 0$ and $w(b) = w_1$. The usual variational approach tells us that $\bar{w}$ will satisfy

$$u_x\bar{w} - 2\nu\bar{w}_{xx} = 0, \quad \bar{w}(0) = 0, \quad \bar{w}(b) = w_1. \tag{2.11}$$

It is clear that, as a function of w, $I_b(w)$ will have no minimum since I_b can be made arbitrarily large and negative by choosing w to be a rapidy oscillating function. Therefore $\bar{w}$ will maximize $I_b(w)$ if (2.11) has a unique solution, that is if the homogeneous equation has only the trivial solution. In addition, the maximum value for I_b will be given by

$$I_b(\bar{w}) = +2\int_0^b \bar{w}(-\frac{1}{2}u_x\bar{w} + \nu\bar{w}_{xx})\, dx - \nu\bar{w}\bar{w}_x|_{-b}^{b} = -2\nu\bar{w}(b)\bar{w}_x(b).$$

The solution of (2.11) can be obtained by solving the initial value problem

$$u_x W - 2\nu W_{xx} = 0, \quad W(0) = 0, \quad W_x(0) = w_2 = w_x(0). \tag{2.12}$$

If $W(b) \neq 0$, then (2.11) has a unique solution and $\bar{w}(x) = w_1\, W(x)/W(b)$. We make the change of variables

$$y = \frac{xM}{2\nu}, \quad U(y) = \frac{u(2\nu y/M)}{M}, \quad W' = \frac{M}{2\nu w_2}\, W(2\nu y/M) \;\; (w_2 \neq 0)$$

to give

$$W'_{yy} - U_y W' = 0, \quad W'(0) = 0, \quad W'_y(0) = 1.$$

Using the approximation (2.10) for the shock profile we see that $W' \approx \widetilde{w}$ where $\widetilde{w}$ satifies the equation

$$\widetilde{w}_{yy} + (1 - \tanh^2(y))\widetilde{w} = 0, \quad \widetilde{w}(0) = 0, \quad \widetilde{w}_y(0) = 1. \tag{2.13}$$

This ODE has no parameters and furthermore, $\widetilde{w}_{yy} \to 0$ exponentially fast as $y \to \infty$. We can thus use a numerical approximation to determine an accurate solution to this problem. Figure (5) shows a numerically computed solution of (2.13). It is calculated with the 2nd order accurate scheme

$$\begin{aligned} w_{n+1} &= 2w_n - w_{n-1} - h^2(1 - (\tanh(x_n))^2)w_n, \;\; n = 1, 2, \ldots, \\ w_0 &= 0, \quad w_1 = h. \end{aligned}$$

By a refinement argument (diminishing h) we conclude that

$$\widetilde{w}_y \geq 0.4, \quad \widetilde{w}(y) \geq 0.4y.$$

Therefore $W(b) \neq 0$ and (2.11) has a unique solution. Using this computational argument we get for the original variables

$$\begin{aligned} -\nu\bar{w}(b)\bar{w}_x(b) &\approx -\nu \, (\frac{2\nu w_x(0)}{M})^2 \, \widetilde{w}(\frac{bM}{2\nu}) \, \frac{M}{2\nu} \, \widetilde{w}_y(\frac{bM}{2\nu}) \\ &\leq -\nu \, (\frac{2\nu w_x(0)}{M})^2 \, \frac{M}{2\nu} \, (0.4)^2 \, \frac{bM}{2\nu} \\ &= -\nu b \, (w_x(0))^2 \, (0.4)^2. \end{aligned}$$

Thus

$$\frac{1}{2}\frac{\partial}{\partial t}\|w\|^2 \lessapprox -\nu b \, (w_x(0))^2 \, (0.4)^2 - \int_{\Omega - B} \frac{1}{2} M w^2 + \nu w_x^2 \, dx \, .$$

This last expression shows that the error will decay rapidly when $w_x(0,t)$ is large. As mentioned above, computations show that $w_x(0,t)$ is usually large with w transitioning from its maximum value to its minimum value through a sharp layer at $x = 0$ as shown in figure (2). *If* $w_x(0) = O(\|w\|/\nu)$ (which appears to be most often the case as observed in calculations) then

$$I_b(w) \leq I_b(\bar{w}) \lessapprox -2\nu b \, (w_x(0))^2 \, (0.4)^2 = O(\|w\|^2),$$

and we obtain exponential decay. Periodicially, however, $w_x(0,t)$ becomes small for a short time. When this happens the decay in the error is not as rapid. This explains the oscillations in the error curves of figure (3).

The argument presented here does not require k_c to be extremely large. Our main assumption is that k_c is chosen large enough so that the large-scale determines the basic form of the shock. It thus seems plausible that the error will decrease rapidly even for small values of k_c.

2.2. *Remarks on the general case for Burgers' equation*

Conjecture: Why the large-scale motion can determine small-scales in Burgers' equation: *The large-scale motion determines the basic structure of the characteristics and shocks. The shocks are the fundamental dissipative structures for Burgers' equation. The large scale motion advects perturbations towards the shocks where they are compressed and dissipated by viscous effects.*

Having considered the case of a single shock we now discuss the general situation. Given generic initial conditions the solution to Burgers's equation will in general develop a number

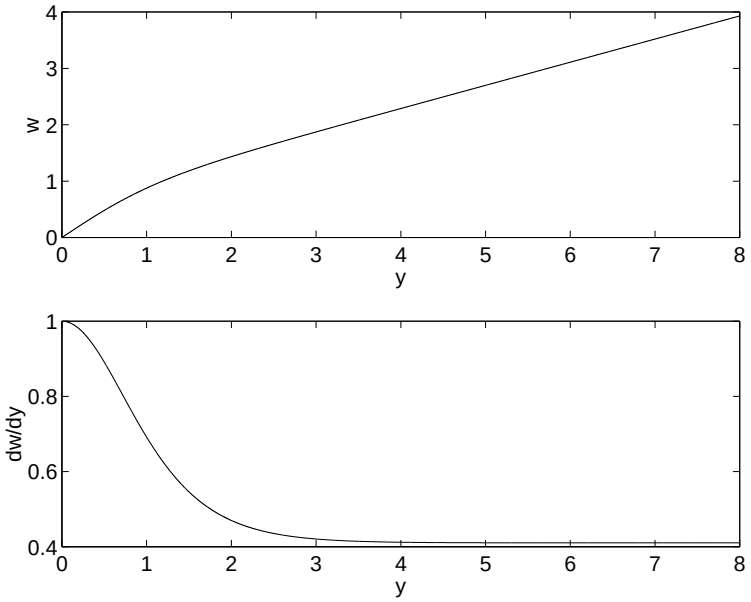

FIGURE 5. Calculated solution to the variational problem (2.13) using $h = .001$. The top figure shows $\widetilde{w}$ and the bottom figure shows $\widetilde{w}_y$.

of shocks of different strengths separated by smooth regions. If the shocks travel with different speeds then after a sufficiently long time only the dominant shock will remain as the smaller shocks are absorbed by the larger shocks. Thus we eventually return to the case of a single shock that was analysed in the previous section. However, we want to know when the small-scale can be reconstructed at earlier times when there are still many shocks present. Given some initial conditions one can predict where and how many shocks will appear by studying the *characteristics*. Given a point (x_0, t_0) in space and time, the characteristic associated with this space-time point is the curve, $X(t;\ x_0, t_0)$, generated by the solution to the nonlinear ordinary differential equation

$$X(t;\ x_0, t_0) \ \ : \ \ \frac{dX}{dt} = u(X, t), \quad X(t_0) = x_0.$$

If we consider the behaviour of two nearby characteristics beginning at x_0 and $x_0 + \delta x_0$ then the equation for the difference $X_\delta = X(t;\ x_0 + \delta x_0, t_0) - X(t;\ x_0, t_0)$ is (for $\delta \to 0$),

$$\frac{dX_\delta}{dt} = \frac{\partial u}{\partial x}(X, t)\ X_\delta, \quad X_\delta(t_0) = x_0.$$

This equation shows that the characteristics will locally converge where $\partial u/\partial x < 0$ and diverge where $\partial u/\partial x > 0$. Shocks will form where the characteristics of nearby points are converging, that is if $\partial u/\partial x < 0$.

If we want the playback solution to generate a shock that appears in the full solution then we should choose k_c large enough so that the characteristics associated with the large scale,

$$X^I(t; x_0, t_0) \ \ : \ \ \frac{dX^I}{dt} = u^I(X^I, t), \quad X^I(t_0) = x_0.$$

also converge. This can be accomplished if we require that in smooth regions of the flow the error in $\partial u/\partial x - \partial u^I/\partial x$ is small. For a time each shock will develop by itself with little influence from distant shocks and thus we can expect that the behaviour of an isolated shock will be similiar to that previously found for a single shock. The assumption we have made is

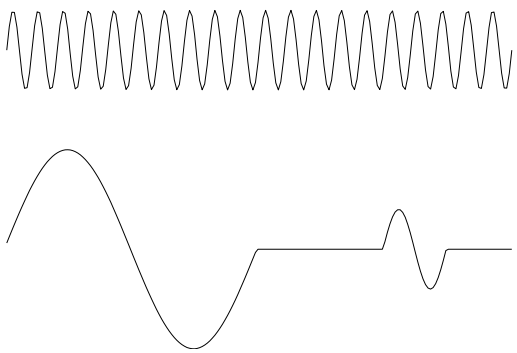

FIGURE 6. Burgers' equation: Two situations when the large-scale will not determine the small-scale are (top) when there is no large-scale and (bottom) when a small-scale feature is isolated from the large scale.

that the flow is smooth between the shocks and that the characteristics through any point (x_0, t_0) will trace a path that intersects a shock that has been created by the large-scale. Errors located at (x_0, t_0) will be advected along the characteristics into the shock where they will be dissipated.

We cannot always expect that small-scale features will be reconstructed from the large-scale, figure (6). Consider the case when the initial conditions (on the interval [-1,1]) consist of a high frequency oscillation,

$$u(x, 0) = \sin(N\pi x), \quad N \gg 1$$

This initial condition will develop into a set of N shocks and the Fourier expansion of the solution will never contain any frequency $k < N$. When $k_c < N$ the large scale will be $u^I(x, t) = 0$ for all time and we will never recover the small-scale by our reconstruction procedure. Similiarly if we have an isolated small shock that is far from the influence of the characteristics of large-scale shocks then we cannot expect to recover it.

In summary, for a given value of k_c and for general initial conditions we can only expect to recover the small scale features that are *coupled* to the large scale but not those small scale features that uncoupled to the large scale. In physical space on can, lossely speaking, think of features being coupled through the characteristics. In Fourier space on can think of small-scale and large-scale features being coupled through the nonlinear term uu_x in Burgers' equation. Given the large-scale Fourier modes this coupling will constrain the small-scale modes.

2.3. *Numerical results for Burgers' equation*

We have solved Burgers' equation numerically using a pseudo-spectral method in space and a fourth-order Runge-Kutta method in time. We compute periodic solutions on the interval $[-1, 1]$. We choose a large number of grid points, $N = O(|u(\cdot, 0)|_\infty/\nu)$ so that the solution is well resolved. For example, for the solutions computed with $\nu = .0125$ we used $N = 2048$, and verified the answers by computing with $N = 1024$ and $N = 4096$. No artificial dissipation is added except that a small number of the highest frequency modes are set to zero at each time step.

We solve Burgers' equations with initial conditions consisting of a sine wave

$$f(x) = -\sin(\pi x).$$

From this initial condition the solution develops into a single N-wave, see figure (2). We define u_r (reference solution) to be the numerical solution to the full equations (2.1a). We define u_p (playback solution) to be the numerical solution to the perturbation equations (2.3). u_p will be a

function of the number of modes, k_c, that we keep in the large-scale. The playback computation is started at time $t = .5$ after the shock has formed. Figure (2) shows the error $w = e_r - e_p$ at time $t = 3$ for $\nu = .00125$. Notice how the error consists of smooth regions away from the the shock position $x = .5$ and a large spike at the shock, consistent with our heuristic description.

We compute the relative error in the playback solution, u_p, compared to the reference solution u_r:

$$e_p(t) = \|u_r^{II} - u_p^{II}\|^2 / \|u_r^{II}\|^2 \quad \text{(relative error in the playback solution)}.$$

We also compute the percentage of the energy that is contained in the large-scale,

$$\mathcal{E}(k_c, t_0) = \frac{\|u^I(\cdot, t_0)\|^2}{\|u(\cdot, t_0)\|^2} \times 100\%.$$

Figure (3) shows the relative errors for different values of ν and different values of k_c. The errors are plotted on a semi-log scale and the results indicate that on average $e_p(t)$ decays exponentially fast. Even for small values of k_c the relative error becomes quite small. Although not shown, the maximum norm errors decay in a similar way. The errors shown in figure (3) do not decay in a uniform manner. The reason for this is explained in section 2.1. More numerical results for Burgers' equation can be found in the report Henshaw *et al.* (2001).

3. The Navier–Stokes equations

We now turn to a discussion of the Navier-Stokes equations. By taking the inner product of $\boldsymbol{u}$ with the momentum equations and integrating by parts one obtains the following estimate for the energy (valid in two and three-dimensions)

$$\frac{1}{2}\frac{d}{dt}\|\boldsymbol{u}\|^2 = -\nu\|\boldsymbol{\nabla u}\|^2. \tag{3.1}$$

In two dimensions a similar procedure can be applied to the Helmholtz vorticity equation to give

$$\frac{1}{2}\frac{d}{dt}\|\xi\|^2 = -\nu\|\boldsymbol{\nabla}\xi\|^2 \quad \text{(two-dimensions only)}. \tag{3.2}$$

In addition, in two-dimensions, the vorticity satisfies a maximum principle,

$$|\xi(\cdot, t)|_\infty \le |\xi(\cdot, 0)|_\infty.$$

These conditions on ξ are strongly related to the fact that solutions to the two-dimensional equations are different in a number of ways from solutions to the three-dimensional equations. For example, in two-dimensions $|\boldsymbol{\nabla u}(\cdot, t)|_\infty$ is essentially bounded by it initial value and thus the energy, $\|\boldsymbol{u}(\cdot, t)\|^2$ decays very slowly since the right-hand-side of equation (3.1), $\nu\|\boldsymbol{\nabla u}\|^2$, remains $O(\nu)$ (here we assume the equations are scaled so that ν is just the inverse of the Reynolds number). Two-dimensional computations show that $\nu\|\boldsymbol{\nabla}\xi\|^2$ can grow to be order $\|\xi\|^2$ when the flow is maximally dissipative (corresponding to a k^{-3} power law for the energy) and thus the enstrophy, $\|\xi\|^2$, can decay exponentially fast resulting in the formation of large coherent structures, see for example McWilliams (1984) and Henshaw *et al.* (1989). In three-dimensions the velocity gradients can grow, apparently to be $O(\nu^{-1/2})$, so that the energy will decay rapidly when there are many dissipative structures in the flow. As a result there can remain a finite viscous dissipation of energy even as the viscosity goes to zero as discussed by Orszag (1970) and Batchelor (1953). Loosely speaking the vorticity ξ and enstrophy $\|\xi\|^2$ are the important variables in 2D corresponding to velocity $\boldsymbol{u}$ and energy $\|\boldsymbol{u}\|^2$ in 3D.

The small-scale of the Navier–Stokes equations, $\{\boldsymbol{u}^{II}, p^{II}\}$, satisfies equation (1.4). The playback solution $\{\boldsymbol{u}_p^{II}, p_p^{II}\}$ satisfies equation (1.6). By subtracting these two equations it follows

that the error between the full solution and the playback solution, $\{\boldsymbol{w}, q\} = \{\boldsymbol{u}^{II} - \boldsymbol{u}_p^{II}, p^{II} - p_p^{II}\}$, satisfies

$$\boldsymbol{w}_t + \mathcal{P}^{II}\left[(\boldsymbol{u}\cdot\boldsymbol{\nabla})\boldsymbol{w} + (\boldsymbol{w}\cdot\boldsymbol{\nabla})\boldsymbol{u} - (\boldsymbol{w}\cdot\boldsymbol{\nabla})\boldsymbol{w}\right] + \boldsymbol{\nabla} q = \nu\Delta\boldsymbol{w}. \tag{3.3}$$

with $\boldsymbol{\nabla}\cdot\boldsymbol{w} = 0$ and with initial conditions

$$\boldsymbol{w}(\boldsymbol{x}, 0) = \boldsymbol{f}^{II}(\boldsymbol{x}).$$

We define the relative error in the playback solution to be

$$e_p(t) = \frac{\|\boldsymbol{u}^{II}(\cdot,t) - \boldsymbol{u}_p^{II}(\cdot,t)\|^2}{\|\boldsymbol{u}^{II}(\cdot,t)\|^2} = \frac{\|\boldsymbol{w}(\cdot,t)\|^2}{\|\boldsymbol{u}^{II}(\cdot,t)\|^2}.$$

As for Burgers' equation we use energy estimates to obtain a bound on the cut-off wave number, k_c, so that the absolute error in the small-scale will decay to zero.

PROPOSITION 2. *The error in the small-scale solution to the Navier-Stokes equations will decay to zero provided we choose the cut-off wavenumber k_c according to*

$$k_c > \sqrt{\frac{\alpha + K_d\overline{|\boldsymbol{\nabla}\boldsymbol{u}|}_\infty}{\nu}}. \tag{3.4}$$

for any $\alpha > 0$, where $K_d = 2$ for two-dimensions and $K_d = 3$ for three-dimensions. In particular we have the result that

$$\|\boldsymbol{w}(\cdot,t)\| \le \mathrm{e}^{-\alpha t}\|\boldsymbol{w}(\cdot,0)\| \ .$$

Here

$$\overline{|\boldsymbol{\nabla}\boldsymbol{u}|}_\infty = \sup_{t\ge 0} |\boldsymbol{\nabla}\boldsymbol{u}(\cdot,t)|_\infty \ . \tag{3.5}$$

Proof:

The proof follows in a similar fashion to the argument for Burgers' equation. We take the inner product of $\boldsymbol{w}$ with equation (3.3) giving

$$(\boldsymbol{w}, \boldsymbol{w}_t) + (\boldsymbol{w}, \mathcal{P}^{II}\left[(\boldsymbol{u}\cdot\boldsymbol{\nabla})\boldsymbol{w} + (\boldsymbol{w}\cdot\boldsymbol{\nabla})\boldsymbol{u} - (\boldsymbol{w}\cdot\boldsymbol{\nabla})\boldsymbol{w}\right] + (\boldsymbol{w}, \boldsymbol{\nabla} q) = \nu(\boldsymbol{w}, \Delta\boldsymbol{w}).$$

We can eliminate the projection $\mathcal{P}^{II}$ since $\boldsymbol{w} = \mathcal{P}^{II}\boldsymbol{w}$ and use integration by parts to give

$$\frac{1}{2}\frac{d}{dt}\|\boldsymbol{w}\|^2 + (\boldsymbol{w}, (\boldsymbol{w}\cdot\boldsymbol{\nabla})\boldsymbol{u}) = -\nu\|\boldsymbol{\nabla}\boldsymbol{w}\|^2$$

Here we have used $(\boldsymbol{w}, (\boldsymbol{u}\cdot\boldsymbol{\nabla})\boldsymbol{w}) = 0$, $(\boldsymbol{w}, q) = 0$ and $(\boldsymbol{w}, (\boldsymbol{w}\cdot\boldsymbol{\nabla})\boldsymbol{w}) = 0$. For example

$$\begin{aligned}
(\boldsymbol{w}, (\boldsymbol{u}\cdot\boldsymbol{\nabla})\boldsymbol{w}) &= \sum_{m=1}^{3}(w_m, u\partial_x w_m + v\partial_y w_m + w\partial_z w_m) \\
&= \frac{1}{2}\sum_{m=1}^{3}(u, \partial_x(w_m^2)) + (v, \partial_y(w_m^2)) + (w, \partial_y(w_m^2)) \\
&= -\frac{1}{2}\sum_{m=1}^{3}(u_x + v_y + w_z, w_m^2) \\
&= 0 \ .
\end{aligned}$$

We can estimate the term $(\boldsymbol{w}, (\boldsymbol{w}\cdot\boldsymbol{\nabla})\boldsymbol{u})$ in the above equation using the crude bound

$$|(\boldsymbol{w}, (\boldsymbol{w}\cdot\boldsymbol{\nabla})\boldsymbol{u})| \le K_d|\boldsymbol{\nabla}\boldsymbol{u}|_\infty\|\boldsymbol{w}\|^2 \ ,$$

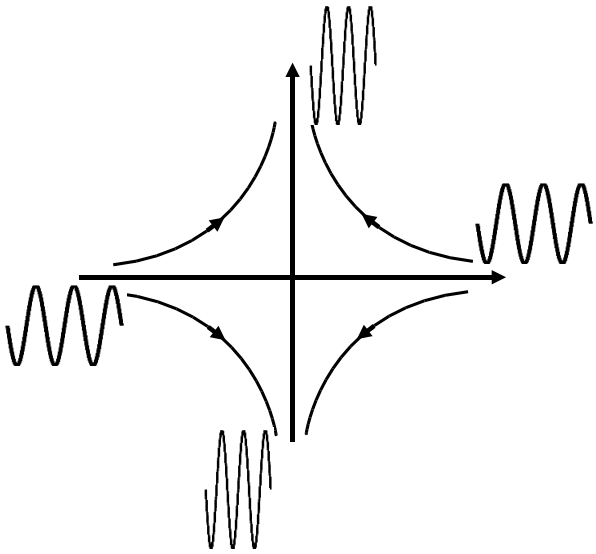

FIGURE 7. This figure illustrates a mechanism for the removal of errors in the playback solution for the Navier-Stokes equations. In certain regions, the large-scale motion will locally advect the errors toward the dissipative structures, such as shear layers. The figure shows a converging flow modeled by the large-scale motion $\boldsymbol{u}^I = (-Ux, Uy, 0)$. An analysis shows that as the errors are advected, energy is transformed into higher frequencies that can be more effectively damped by the viscous dissipation. The nonlinear coupling between the large- and small-scale motion can thus increase the effective dissipation of the error.

where $K_d = 2$ for two-dimensions and $K_d = 3$ for three-dimensions. Since the Fourier coefficients of $\boldsymbol{w}$ are zero for $|k| \le k_c$ it follows that $\|\boldsymbol{\nabla w}\|^2 \ge k_c^2 \|\boldsymbol{w}\|^2$ and thus

$$\frac{1}{2}\frac{d}{dt}\|\boldsymbol{w}\|^2 \le (K_d|\boldsymbol{\nabla u}|_\infty - \nu k_c^2)\|\boldsymbol{w}\|^2 \ .$$

Therefore by choosing the cut-off wave number to be

$$k_c \ge \sqrt{\frac{\alpha + K_d|\boldsymbol{\nabla u}|_\infty}{\nu}}$$

then

$$\frac{1}{2}\frac{d}{dt}\|\boldsymbol{w}\|^2 \le -\alpha\|\boldsymbol{w}\|^2 \ .$$

and it follows that the error will decay exponentially fast,

$$\|\boldsymbol{w}(\cdot,t)\| \le \mathrm{e}^{-\alpha t}\|\boldsymbol{w}(\cdot,0)\|.$$

Unfortunately these estimates do not indicate that the relative error in the small-scale approaches zero.

Computations presented in later sections suggest that the estimate (3.4) for the cutoff wave number is often much too large. For example, for two-dimensional computations with $\nu = 2.5 \times 10^{-6}$ and $|\boldsymbol{\nabla u}|_\infty = 1$ instead of $k_c \approx 900$ as predicted by (3.4) we instead find that $k_c \approx 16$ is large enough, see figure (12).

3.1. *Remarks*

We can give a heuristic argument as to why the errors may decay more rapidly than predicted by the energy proof. The equation for the error in the playback solution

$$\boldsymbol{w}_t + \mathcal{P}^{II}\left[(\boldsymbol{u}\cdot\boldsymbol{\nabla})\boldsymbol{w} + (\boldsymbol{w}\cdot\boldsymbol{\nabla})\boldsymbol{u} - (\boldsymbol{w}\cdot\boldsymbol{\nabla})\boldsymbol{w}\right] + \boldsymbol{\nabla} q = \nu\Delta\boldsymbol{w}\ , \tag{3.6}$$

is very similar in form to the equation for the error (2.4*b*) for Burgers' equation. As with Burgers' equation the behaviour of the solutions to the Navier–Stokes are strongly dependent on the characteristics,

$$\frac{d\boldsymbol{X}}{dt} = \boldsymbol{u}(\boldsymbol{X},t), \quad \boldsymbol{X}(t_0) = \boldsymbol{x}_0.$$

and the variation of the characteristics,

$$\frac{d\boldsymbol{X}_\delta}{dt} = \frac{\partial \boldsymbol{u}}{\partial \boldsymbol{x}}(\boldsymbol{X},t)\ \boldsymbol{X}_\delta(\boldsymbol{x},t)\ =\ \begin{bmatrix} u_x & u_y & u_z \\ v_x & v_y & v_z \\ w_x & w_y & w_z \end{bmatrix} \boldsymbol{X}_\delta(\boldsymbol{x},t).$$

Let λ_m, $m = 1,2,3$ denote the eigenvalues of the Jacobian matrix $\partial\boldsymbol{u}/\partial\boldsymbol{x}$. The sum of the eigenvalues is equal to the trace of the Jacobian matrix which equals zero since the flow is incompressible. Consider the real parts of the eigenvalues, $Re(\lambda_m)$. If the real parts are not all zero then since their sum is zero we either have one eigenvalue with negative real part and two with non-negative real part or two eigenvalues with negative real part and one with non-negative real part. If we start from smooth initial conditions then when $Re(\lambda_1) < 0$ and $Re(\lambda_{2,3}) \geq 0$ the characteristics will converge in the direction of the first eigenvector and diverge in the directions of the other two. Neglecting the stretching term $(\boldsymbol{\xi}\cdot\boldsymbol{\nabla})\boldsymbol{u}$, the directional-derivatives of the vorticity will tend to increase in the direction of the first eigenvector and decrease in the other two. The solution will thus locally attempt to form a shear layer. In the other case when $Re(\lambda_{1,2}) < 0$ and $Re(\lambda_3) \geq 0$ (which can only happen in three dimensions) the characteristics will converge in two directions and diverge in the third, while the derivatives of the vorticity will increase in two directions and decrease in the third. This corresponds to the formation of a vortex filament. When the real parts of the eigenvalues are all zero then the characteristics neither converge nor diverge, if the imaginary parts are non-zero then this corresponds to a rotating flow, such as in a large vortex blob.

There are two important points to be made here. One is that the characteristics, which are mainly defined by the the large-scale, cause the formation of the dissipative structures where the gradients of vorticity are large. The second is that the characteristics will often advect the errors in the playback solution into these dissipative structures.

If we want the large-scale to determine the formation of the dissipative structures then we should choose k_c large enough so that the Jacobian matrix of the large scale, $\partial\boldsymbol{u}^I/\partial\boldsymbol{x}$ is a good approximation to the Jacobian-matrix $\partial\boldsymbol{u}/\partial\boldsymbol{x}$ of the full solution for then the large-scale will represent the characteristics reasonably well.

Unlike the shocks that form in solutions to Burgers' equation, which are very stable dissipative structures, the shear layers and vortex filaments are unstable to perturbations and will tend to stretch and roll up forming more complicated structures and small vortex blobs, see Bell & Marcus (1992) and Saffman (1992). These fine scale features are probably very effective at dissipating energy. However it is not apparent from arguments based on characteristics that the internal details of these unstable dissipative structures would be reconstructed in the playback solution. Surprisingly the numerical computations show that many of these details are reconstructed, see the contour plots of the playback solution in figure (12) for two-dimensions and figure (19) for three-dimensions. It is likely that the nonlinear terms in the Navier-Stokes equations which couple the small-scale Fourier modes to the large-scale Fourier modes have a strong

effect in the dissipative structures. This effect is hard to quantify but it is consistent with our previous calculations that show perturbations to the small scale are quickly damped, see Henshaw & Kreiss (1991), Browning *et al.* (1998*a*) and Kreiss & Yström (1998).

As in the case for Burgers' equation there will be situations when the large scale will not determine the small-scale such as if there is no large-scale or if there are isolated regions of the flow that are only weakly connected to the large scale.

Conjecture: Why the large scale motion often determines the small scale for the Navier-Stokes: *The large-scale modes determine the basic structure of the flow and sets up the dissipative structures. In two-dimensions the main dissipative structures appear to be shear layers while in three-dimensions the dissipative structures appear to be the highly convoluted vortex filaments and shear layers, Lesiuer (1990), Chorin (1994). The large scale motion advects perturbations towards the dissipative structures where they are compressed and transformed into higher frequencies which can be effectively dissipated by viscous effects.*

4. Calculations of the two-dimensional Navier–Stokes equations

In this section we describe numerical results for the two-dimensional Navier-Stokes equations. We solve the two-dimensional Navier-Stokes equations for the third component of the vorticity, $\omega = \xi_3$,

$$\omega_t + (\boldsymbol{u}\cdot\boldsymbol{\nabla})\omega = \nu\Delta\omega$$
$$\boldsymbol{\nabla}\cdot\boldsymbol{u} = 0$$

with a pseudo-spectral method in space and and a fourth-order predictor-corrector method in time, see Henshaw *et al.* (1989) for more details. We define the kinetic energy spectrum $E(k)$ as

$$E(k) = \frac{1}{2}\sum_{k-1/2\le|\boldsymbol{k}|<k+1/2} |\hat{\boldsymbol{u}}(\boldsymbol{k},t)|^2.$$

and thus

$$E_K = \|\boldsymbol{u}\|^2/(2\mathcal{V}) = \frac{1}{2}\sum_{\boldsymbol{k}} |\hat{\boldsymbol{u}}(\boldsymbol{k},t)|^2 = \sum_k E(k).$$

We also define the an averaged vorticity spectrum, $\hat{w}(k)$ defined by

$$\hat{w}(k) = \frac{\sum_{|\boldsymbol{l}-\boldsymbol{k}|<1/2} |\hat{\omega}(\boldsymbol{l})|}{\sum_{|\boldsymbol{l}-\boldsymbol{k}|<1/2} 1}.$$

The initial conditions for the reference solution, $\omega_r(\boldsymbol{x},t)$, are chosen to have random phase and an energy spectrum of

$$E_r(k) = C_r\, k\, e^{-(k/k_a)^2}$$

where $k_a = 3.5$ and the constant C_r is chosen so that the vorticity has a maximum of 1,

$$|\omega_r(\cdot,\cdot,0)|_\infty = 1.$$

The maximum value of the velocity in the reference run is about 0.2, the average value for the velocity is about $u_C = 1/10$ thus the convective time scale is about $t_C = 2\pi/u_C \approx 60$. We solve with N grid points corresponding to $N/2$ Fourier modes. We use $N = 256, 512$ and 1024 for $\nu = 10^{-4}$, 10^{-5} and 2.5×10^{-6}, respectively. Figure 8 shows some results for the reference computation with $\nu = 2.5\times10^{-6}$. Notice that the energy is almost constant and that the rate of dissipation of enstrophy is a maximum at about time $t = 70$.

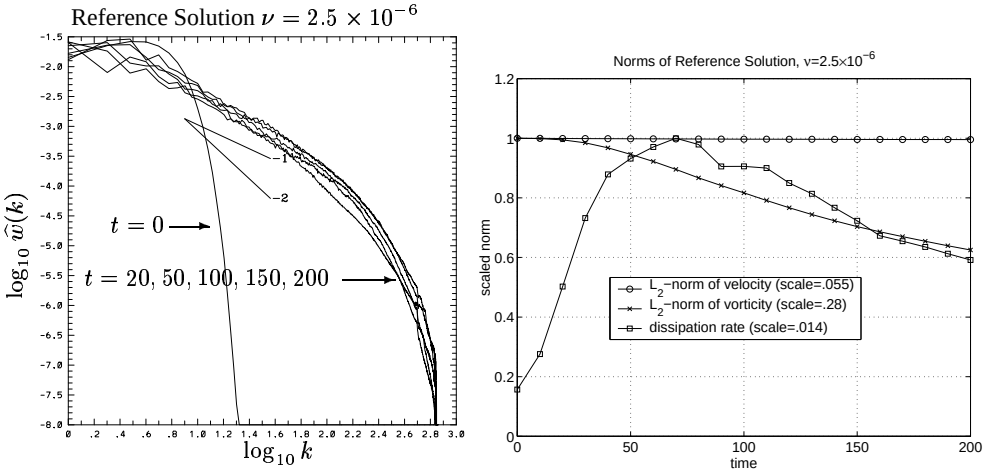

FIGURE 8. Two-dimensional Navier-Stokes: data for the reference solution. Left: spectrum of the vorticity. Right: The scaled L_2-norm of the velocity ($\circ$), scaled L_2-norm of the vorticity ($\times$) and scaled dissipation rate $\sqrt{\nu}\|\boldsymbol{\nabla} w\|$ ($\square$). The quantities on the right are scaled to have a maximum of 1. The play-back solution begins at time $t = 50.$ when $\|\boldsymbol{\nabla} w\|$ is nearly a maximum. The energy only decreases by $.45$ percent by time $t = 200.$

We define the *playback solution,* $\omega_p(\boldsymbol{x}, t; k_c) = \omega_p^I + \omega_p^{II}$ to be solution of the equations when the first k_c modes are set equal to those from the reference solution for all time, $\omega_p^I(\boldsymbol{x}, t) = \omega_r^I(\boldsymbol{x}, t)$, but having zero initial conditions for the small-scale, $\omega_p^{II}(\boldsymbol{x}, t_0) = 0$. The small-scale of the playback solution is computed from the equations analogous to (1.4). In practice we solve for all Fourier modes but replace, at each time step, the large-scale modes with those computed from the reference calculation.

We define the *truncated solution* $\omega_\tau(\boldsymbol{x}, t; k_c)$ to be the solution to the full equations with initial conditions $\omega_\tau^I(\boldsymbol{x}, t_0) = \omega_r^I(\boldsymbol{x}, t_0)$, and $\omega_\tau^{II}(\boldsymbol{x}, t_0) = 0$. Thus the first k_c modes in truncated solution are given as initial conditions but are NOT assigned over time. We will see that the truncated solution diverges from the reference solution while the playback solution does not. The playback and truncated computations were both started at $t_0 = 50$.

The relative error in the playback solution is defined as

$$e_p(t) = \frac{\|\omega_p^{II} - \omega_r^{II}\|^2}{\|\omega_r^{II}\|^2},$$

with a similar definition for the relative error in the truncated solution, $e_\tau(t)$. We also compute the percentage of the enstrophy that is contained in the large-scale,

$$\mathcal{E}(k_c, t) = \frac{\|\omega^I(\cdot, t)\|^2}{\|\omega(\cdot, t)\|^2} \times 100\%.$$

In figure (9) we summarize the two-dimensional results for errors in the playback solution. The figures show the relative errors for different values of the cut-off wave number k_c and different values of ν. The results show that a relatively few number of modes are required for the relative error to decrease. The error decreases more rapidly as k_c is increased. As ν is decreased somewhat more modes are required to attain the same relative error. The bottom right sub-figure of (9) shows that the relative errors for different values of ν is roughly correlated with the percentage of vorticity in the large scale, $\mathcal{E}(k_c, t = 150)$. For $\mathcal{E}(k_c, t = 150) = 80\%$ the the relative error lies between $5 - -15\%$. Figure (10) shows corresponding results for the truncated solution

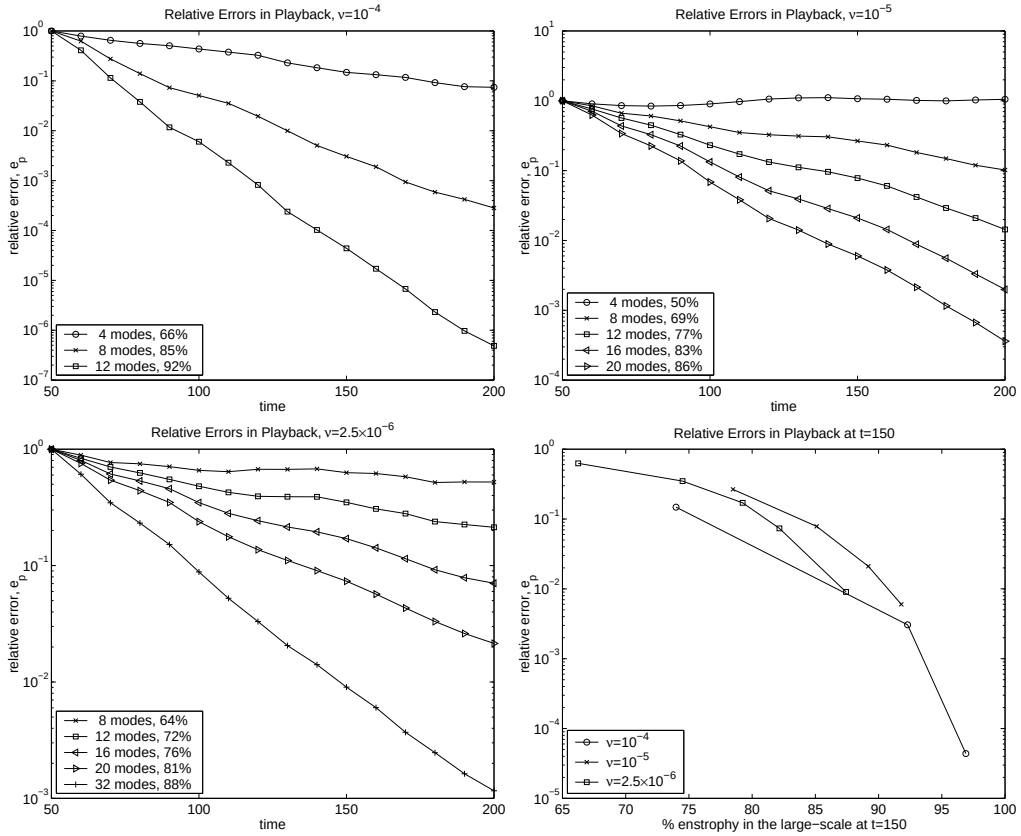

FIGURE 9. Two-dimensional Navier-Stokes: the relative errors in the high modes for the playback solutions as a function of time and a function of the cut-off wave number k_c. As k_c is increased the relatives errors decrease. The captions indicate the percentage of enstrophy contained in the large-scale at $t = 50$.

when the time history of the large scale is not assigned over time. In this case the error quickly grows.

Although $e_p(t)$ is a good quantitative measure of the error we also find it useful to compare the vorticity contours of the reference solution to those of the playback solution. This *picture-norm* measure gives one a good indication of when the small scale features, such as small vortices, are recovered. If a small vortex is recovered but in slightly the wrong position then the *picture-norm* may be small while the relative error can be large. Also note that the position of contour lines are a sensitive measure of a function, especially where the function is nearly flat.

Figures (11-12) shows some results comparing the contours of the vorticity for the reference solution to the play-back solution with $k_c = 16$. In each figure we show the the play-back solution on the left and the reference solution on the right.The initial conditions for the play-back solution are taken from the reference solution at time $t = 50$. At the initial time, $t = 50$, figure (11) the two solutions are very different. By time $t = 100$ (not shown) the fine scale features have been recovered to a significant degree and by $t = 200$ they agree to a remarkable degree. In figure (14) we show corresponding results for the truncated solution. Although some of the large scale structures can still be identified the truncated solution is very different from the reference solution.

Figure (13) shows another representation of the errors in the playback and truncated solutions.

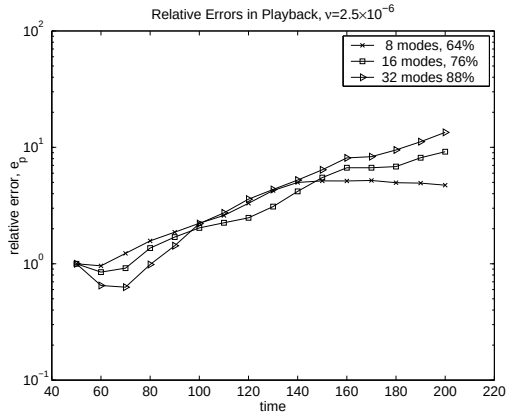

FIGURE 10. Two-dimensional Navier-Stokes: the relative errors in the high modes when the initial conditions are truncated to k_c modes but the lowest k_c modes are NOT assigned over time. The errors initially decrease but then quickly grow.

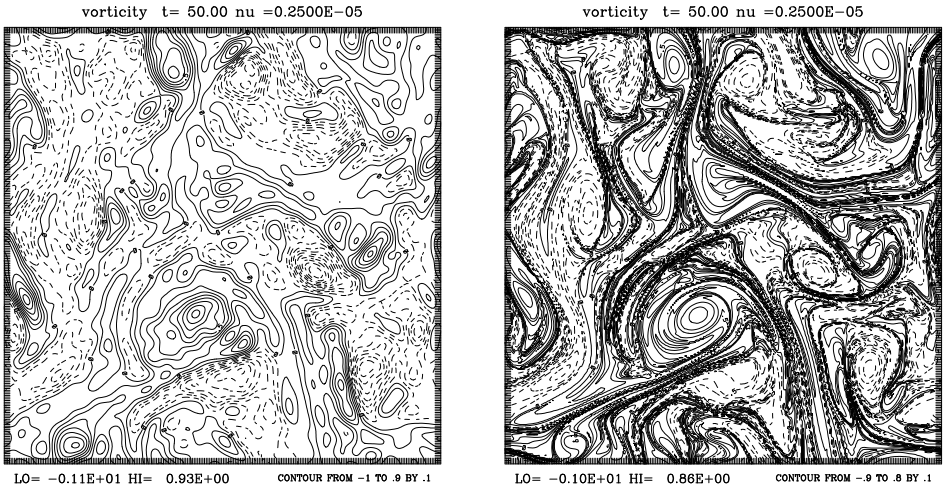

Play-back initial conditions $k_c = 16$. Reference solution.

FIGURE 11. Two-dimensional Navier–Stokes: contours of the vorticity at the starting time for the play-back computation. Left: play-back solution, right: reference solution. The initial conditions for the play-back solution are set equal to the lowest $k_c = 16$ modes of the reference solution at $t = 50$.

Shown are the spectrums of the relative errors. While the error in the playback solution decreases over time those in the truncated solution increase as the errors in the large-scale quickly grow.

More numerical results for the two-dimensional Navier-Stokes equations can be found in Browning *et al.* (1998*b*) and Henshaw *et al.* (2001).

5. Calculations of the three-dimensional Navier–Stokes equations

The three-dimensional numerical results were computed with a de-aliased pseudo-spectral method that was based on a code developed by Lundbladh *et al.* (1992), Hallbäck (1993) and Alvelius (1997). The equations are formulated in terms of the vorticity and velocity in a form where the pressure is eliminated. The primary dependent variables are chosen to be the $y-$components of the vorticity and velocity. From these the x and z components of the velocity and vorticity can

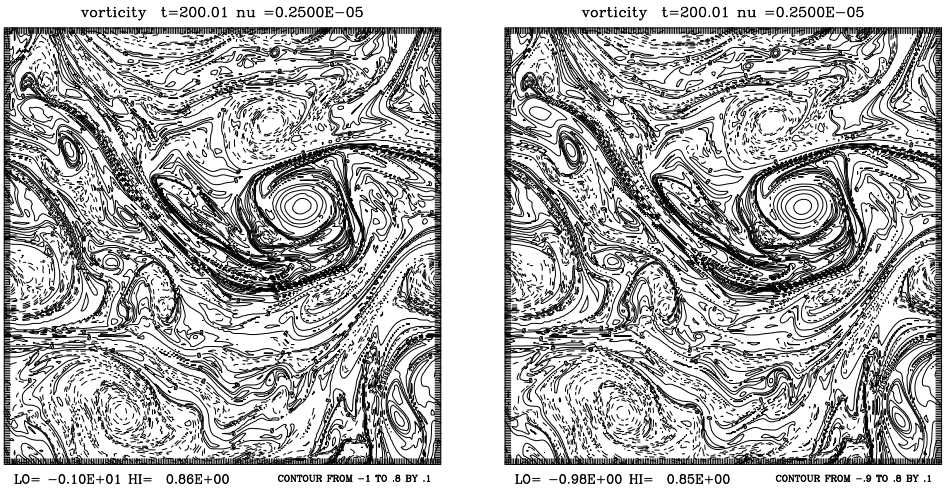

Play-back solution $k_c = 16$. Reference solution.

FIGURE 12. Two-dimensional Navier–Stokes: solutions at time $t = 200$. Left: play-back solution, right: reference solution. The play-back solution is almost the same as the reference solution. Many of the fine scale features have been recovered in a pointwise sense, not just in a statistical sense. The relative error is 7%.

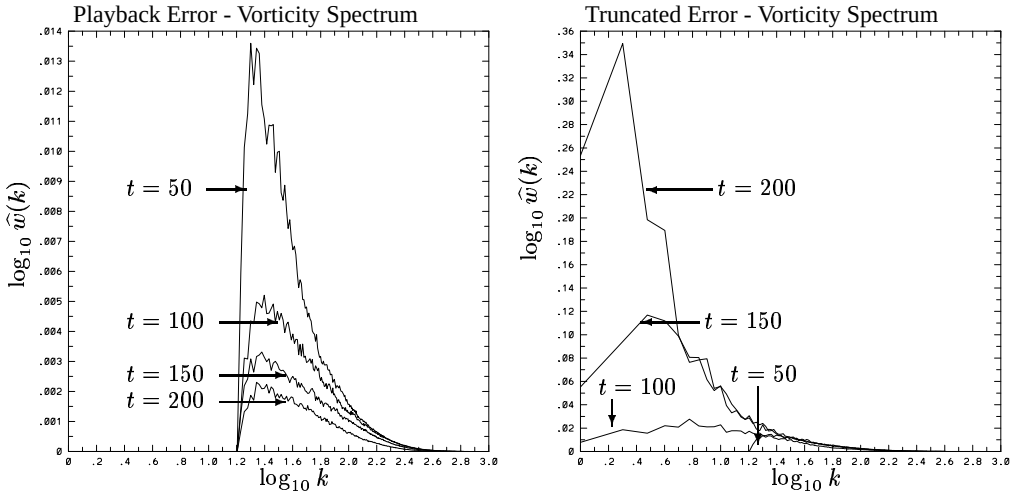

Error when time-history is fixed. Error when time-history is NOT fixed.

FIGURE 13. Two-dimensional Navier–Stokes. Left: The relative error in the vorticity spectrum for the play-back solution with 16 modes given. The errors decrease as time proceeds. Right: The relative error in the spectrum when the full equations are solved with initial conditions truncated to the first 16 modes of the reference solution.

be easily updated since in spectral space the continuity equation and the definition of the vorticity in terms of the velocity are represented as simple algebraic relations. For the discretisation in time, the non-linear terms are treated explicitly with a second order Adams-Bashford method. The second order Crank-Nicholson method is used for the linear viscous term. There is a variable time step feature implemented in the code but since we do comparisons between different calculations at equal simulation times, we use a constant time step.

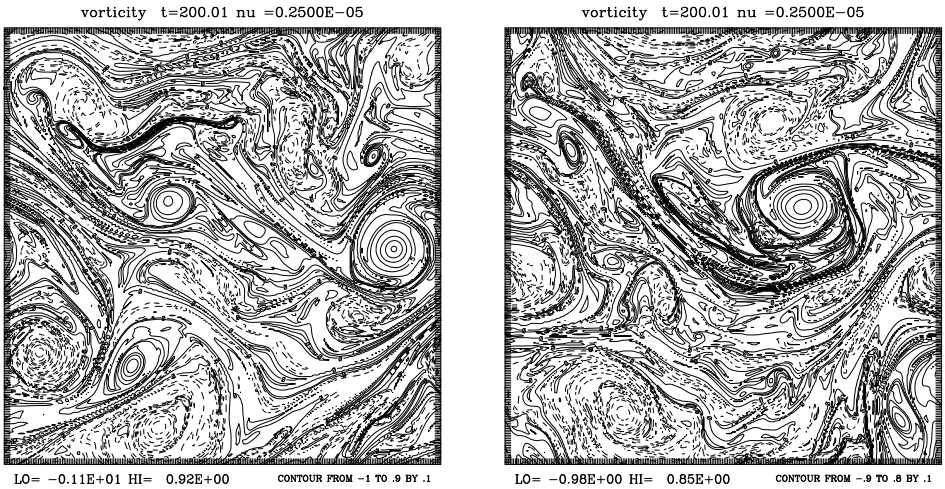

Solution when time-history is NOT fixed. Reference solution.

FIGURE 14. Two-dimensional Navier-Stokes. Left: The solution to the full Navier-Stokes equations at $t = 200$ when the initial conditions are chosen to be the first 16 modes of the reference solution but the time history is NOT enforced as a constraint. Right: reference solution. The solution on the left has clearly changed dramatically in comparison the play-back solution of figure (12)

We consider equal grid spacing in all directions. Let $N = 2^j$ for some $j > 0$, and

$$k_i \in [-N/2 + 1, N/2], \quad \boldsymbol{k} = (k_1, k_2, k_3)^T.$$

We denote the smallest scale that we can represent on the grid by λ^G_{min} and will use the relation

$$\lambda^G_{min} = 1/k_{max} = 2/N.$$

The reference solution for our three-dimensional computations was obtained with a viscosity equal to $\nu = 1/300$ and $N = 256$. We denote this numerical solution by $\boldsymbol{u}_r$ and $\boldsymbol{\xi}_r$ for the velocity and vorticity fields respectively. The initial data for the reference calculation has random phase, satisfy the incompressibility constraint and has the kinetic energy spectrum $E(k) = C_r k^2 e^{-(k/k_0)^2}$, where $k_0 \approx 3.4$ and C_r chosen such that $E_K(\boldsymbol{u}_r(\cdot, 0)) = 0.5$. In figure 15, the kinetic energy, rate of dissipation and the maximum-norm of the vorticity is plotted versus time $t \in [0, 5]$. In figure 16 the energy spectrum at $t = 0.0, 1.0$ and at $t = 1.5, 2.5, 3.5, 4.5$, are plotted respectively. We now ask if the reference calculation is well resolved. Henshaw *et al.* (1990) have shown that the smallest length-scale of the flow is of the order

$$\lambda_{min} \sim (\nu/\overline{|\boldsymbol{\nabla u}|}_\infty)^{\frac{1}{2}}. \tag{5.1}$$

where $\overline{|\boldsymbol{\nabla u}|}_\infty$ is defined in (3.5). Grid refinement calculations were performed by Kreiss & Ystrom (1998) and it was concluded that the inverse of the right hand side of (5.1) is actually a good approximation of how many modes are needed to resolve the solution accurately. For the reference calculation we compute

$$\overline{|\boldsymbol{\nabla u}|}_\infty \approx \max_{t\in[0,5]} |\boldsymbol{\xi}_r|_\infty \approx 47.3,$$

which gives

$$(\nu/\overline{|\boldsymbol{\nabla u}|}_\infty)^{\frac{1}{2}}/\lambda^G_{min} \approx 1.07,$$

and we conclude that the reference calculation is well resolved. For later reference we also com-

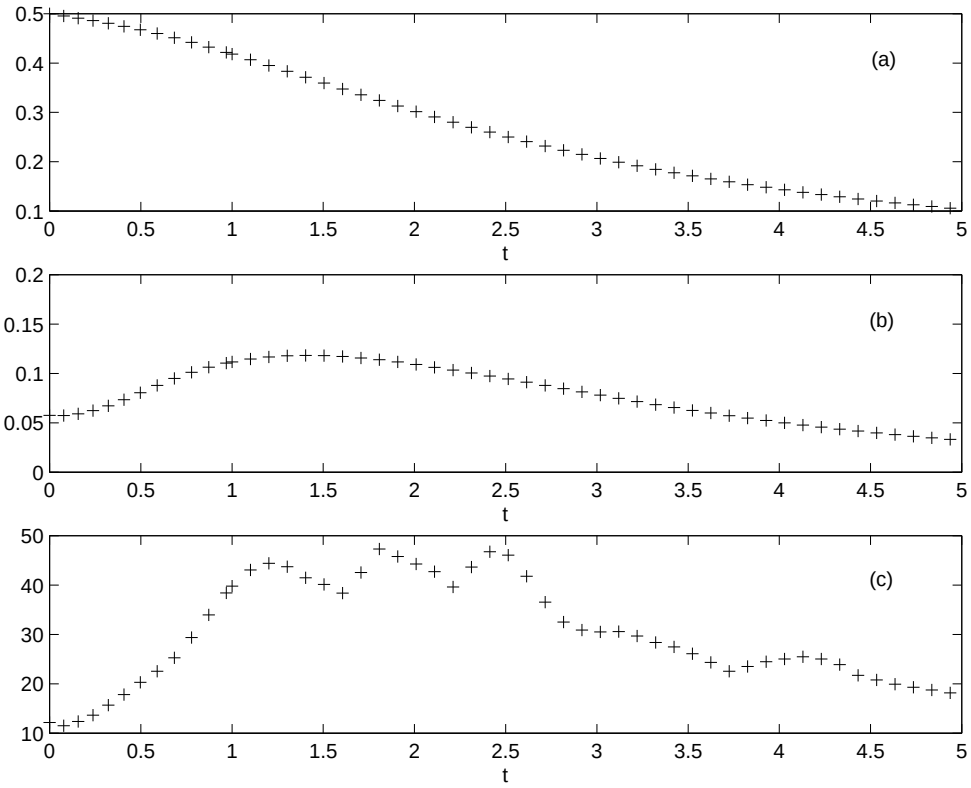

FIGURE 15. Results for the reference solution to the three-dimensional Navier–Stokes equations showing (a) the kinetic energy, E_K, (b) the rate of dissipation of energy: $\epsilon = \nu \|\boldsymbol{\nabla} \boldsymbol{u}_r\|^2 / \mathcal{V}$, and (c): the maximum norm of the vorticity, $|\boldsymbol{\xi}_r|_\infty$.

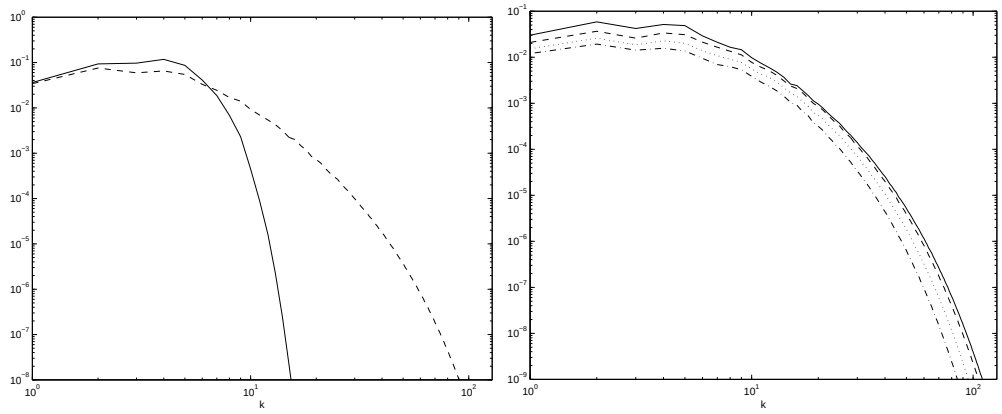

FIGURE 16. Energy spectrum $E(k)$ for the reference solution in three-dimensions, left: solid line $t = 0.0$, dashed $t = 1.0$, right: solid line $t = 1.5$, dashed $t = 2.5$, dotted $t = 3.5$, dashed-dotted $t = 4.5$.

pute the relative kinetic energy and enstrophy contents of the large-scale together with the L_2 norm of $\boldsymbol{F}^{II}(\boldsymbol{u}_r^I)$ for the reference run for $k_c = 8, 10, 12$, see figure 17.

As in the two-dimensional case we define the playback solution $\boldsymbol{u}_p = \boldsymbol{u}_p^I + \boldsymbol{u}_p^{II}$ with the the large-scale motion set equal to the reference solution large-scale motion, $\boldsymbol{u}_p^I(\boldsymbol{x}, t) = \boldsymbol{u}^I(\boldsymbol{x}, t)$

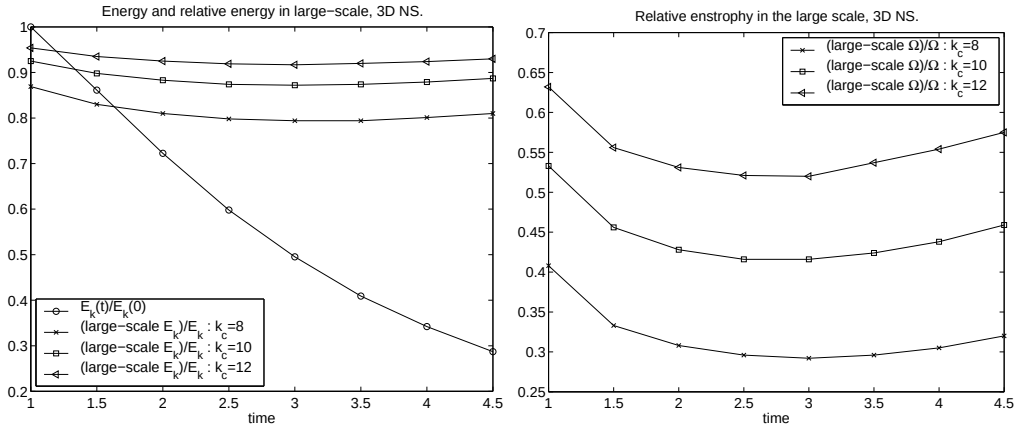

FIGURE 17. Results for the reference solution for computations of the three-dimensional Navier-Stokes equations. Left: relative energy in the large-scale for different values of k_c. Right: relative enstrophy in the large scale for different values of k_c.

and the small-scale computed from (1.6). The playback solution is started at $t_0 = 1.$ and we solve for the three cases $k_c = 8, 10, 12$.

For comparison, or proof of concept, we also make a calculation for the Navier–Stokes problem (1.1) with truncated initial data

$$\boldsymbol{u}_0(\boldsymbol{x}) = \boldsymbol{u}_r^I(\boldsymbol{x}, t_0),$$

where $k_c = 12$ and $t_0 = 1.0$. This numerical solution is denoted $\boldsymbol{u}_\tau$.

In figure (18) we show the relative error in the playback solutions and the truncated solutions. The results are similar to those from the two-dimensional case. The relative error in the playback decreases significantly even when a relatively few number of large-scale modes are specified. In contrast, the errors in the truncated solution quickly grow.

Figure (19) compares contours of $|\boldsymbol{\xi}|$ for the playback and reference solution. The comparisons are done in the $y = y_0$ planes for which $|\boldsymbol{\xi}_r|$ attains its maximum. By time $t = 3$ many of the fine scale features of the solution have been recovered in the playback solutions with $k_c = 12$ giving better results than $k_c = 10$.

More numerical results for the three-dimensional Navier-Stokes equations can be found in Kreiss & Ystrom (1998) and Henshaw *et al.* (2001).

6. Summary

We have attempted to reconstruct the small-scale spatial Fourier modes by incorporating the time history of the first k_c Fourier modes (the large-scale) as known forcing into the equations governing the evolution of the small-scale. We have investigated this process for Burgers' equation in one-dimension and for the incompressible Navier-Stokes equations in two and three dimensions. Numerical computations show that the small-scale features can sometimes be reconstructed to a surprising degree of accuracy even for a relatively few number of large-scale modes. There are, however, situations when the small-scale is uncoupled to the large-scale and cannot be reconstructed. Rigorous analytical results predict a value for k_c which is much larger than those found numerically. We present some non-rigorous analysis to suggest why so few modes are sometimes sufficient. We argue that the characteristics of the large scale flow cause the formation of the dissipative structures, shocks for Burgers equation, shear layers and vortex filaments for the Navier–Stokes. The characteristics also advect errors into the dissipative structures

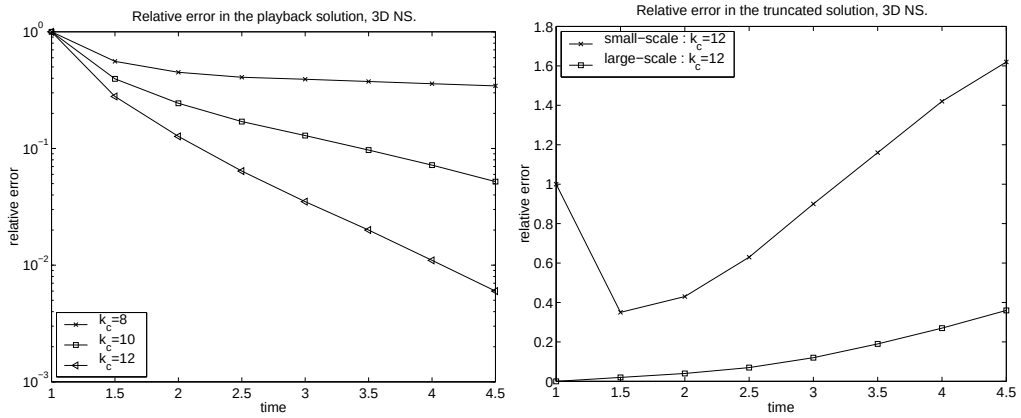

FIGURE 18. Three-dimensional Navier–Stokes. The figure on the left shows the relative error in the playback solution when the cutoff wave number is $k_c = 8, 10, 12$. The relative error is $\|\boldsymbol{u}_r^{II} - \boldsymbol{u}_p^{II}\|^2/\|\boldsymbol{u}_r^{II}\|^2$. The figure on the right shows the relative errors in small-scale and the large-scale for the truncated solution when the large-scale is not assigned over time. The relative small-scale error in the truncated solution is $\|\boldsymbol{u}_r^{II} - \boldsymbol{u}_\tau^{II}\|^2/\|\boldsymbol{u}_r^{II}\|^2$ and the relative error in the large-scale is $\|\boldsymbol{u}_r^{I} - \boldsymbol{u}_\tau^{I}\|^2/\|\boldsymbol{u}_r^{I}\|^2$.

where they are removed by viscous effects. From another viewpoint, the nonlinear terms of the equations can provide a strong coupling between the small-scale Fourier modes and large-scale Fourier modes so that when the large-scale modes are given over time the small-scale modes are constrained to be consistent with the large-scale modes.

This research was supported by the office of Naval research grant no. N00014-93-1-0551; P00005 and no. N00014-98-1-0125. and under the auspices of the U.S. Department of Energy by the University of California, Lawrence Livermore National Laboratory under contract No. W-7405-Eng-48. We would like to thank Dr. Richard Lau at the Office of Naval Research for all the support he has given us over the years. We would like to thank Prof. Arne Johansson for letting us use their computer program and PhD student Krister Alvelius for helping us get started with the code, both at the Department of Mechanics at the Royal Institute of Technology in Stockholm Sweden. We gladly acknowledge many stimulating discussions with Dr. Gerald Browning at CIRA, Colorado State University and NOAA Forecast System Laboratory. The three-dimensional calculations presented here were done at the DoD High Performance Computing Center, Naval Oceanographic Office(NAVO) MSRC on their Cray C90 and T90 PVP systems.

REFERENCES

ALVELIUS, K. 1997 Large eddy simulations of homogeneous turbulence. *Tech. Rep.* 1997:12. Department of Mechanics, Royal Institute of Technology.

BATCHELOR, G. 1953 *The Theory of Homogeneous Turbulence*. Cambridge: Cambridge University Press.

BELL, J. & MARCUS, D. 1992 Vorticity intensification and transition to turbulence in a three-dimensional Euler equations. *Comm. Math. Phys.* **147**, 371–394.

BROWNING, G., HENSHAW, W. & KREISS, H. 1998*a* A numerical investigation of the interaction between the large and small scale of the two-dimensional Navier-Stokes equations. *Tech. Rep.* 98-23. Dep. of Math. University of California.

BROWNING, G., HENSHAW, W. & KREISS, H.-O. 1998*b* A numerical investigation of the interaction between the large and small scales of the two-dimensional incompressible Navier-Stokes equations. Research Report LA-UR-98-1712. Los Alamos National Laboratory.

CHARNEY, J., HALEM, M. & JASTROW, R. 1969 Use of incomplete historical data to infer the present state of the atmosphere. *Journal of Atmospheric Science* **26**, 1160–1163.

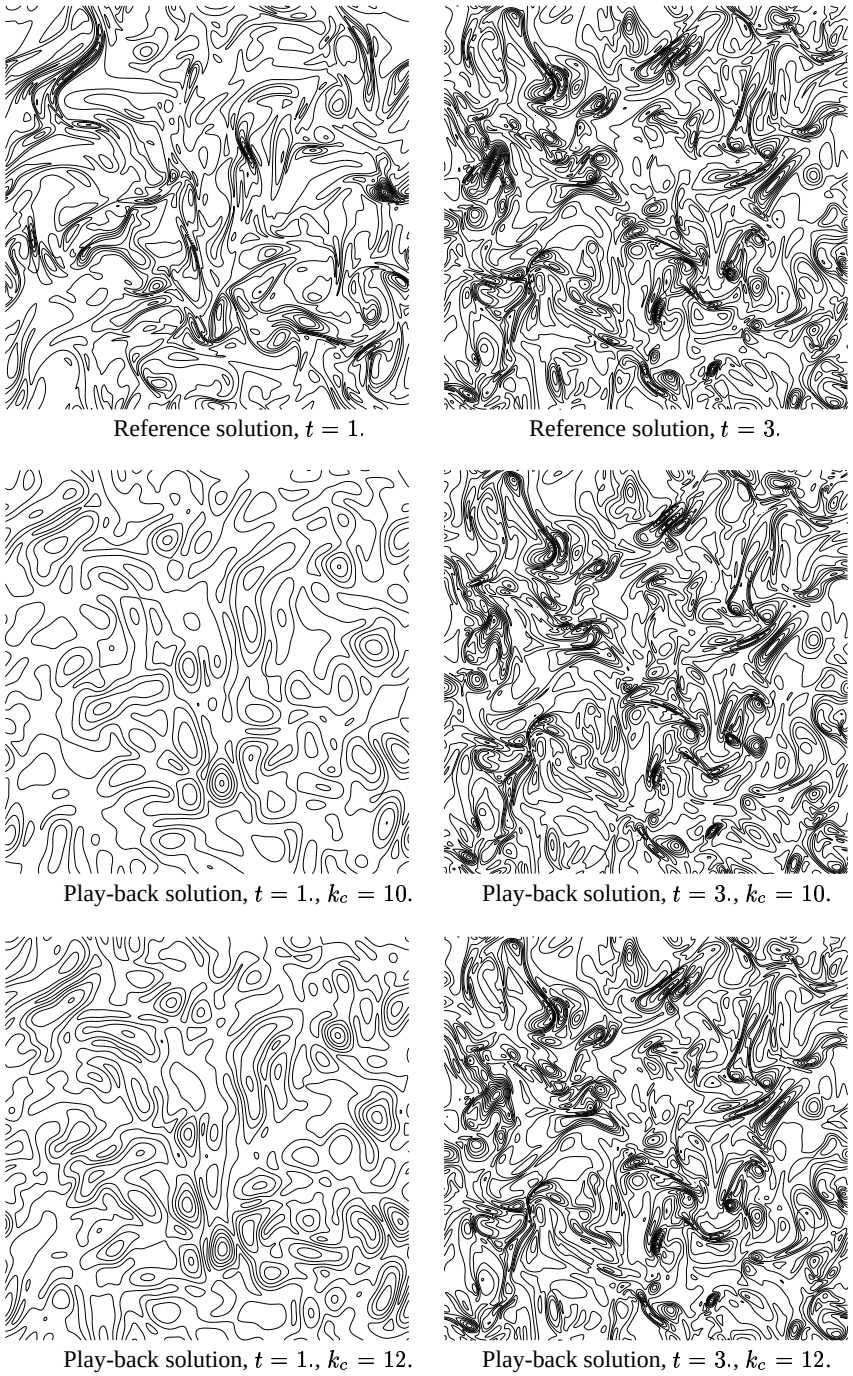

FIGURE 19. Three-dimensional Navier–Stokes: contours of $|\boldsymbol{\xi}|$ for the reference and playback calculations at $t = 1.0$ (left column) and $t = 3.0$ (right column). The comparisons are done in the $y = y_0$ planes for which $|\boldsymbol{\xi}_r|$ attains its maximum. Notice that for $k_c = 12$ (relative error of 19%), many of the fine details of the solution have been recovered by $t = 3$. The agreement for $k_c = 10$ (relative error 19%) is also fairly good.

CHORIN, A. J. 1994 *Vorticity and Turbulence*. New York: Springer Verlag.

CHORIN, A. J., KAST, A. & KUPFERMAN, R. 1999 Unresolved computation and optimal predictions. *Comm. Pure Appl. Math* **52**, 1231–1254.

CONSTANTIN, P., DOERING, C. & TITI, E. 1996 Rigorous estimates of small scales in turbulent flows. *J. Math. Phys.* **37** (12), 6152–6156.

CONSTANTIN, P., FOIAS, C., MANLEY, P. & TEMAM, R. 1985 Determining modes and fractal dimensions of turbulent flows. *J. Fluid. Mech.* **150**, 427–440.

CONSTANTIN, P., FOIAS, C. & TEMAM, R. 1984 Attractors representing turbulent flows. *Mem. Am. Math. Soc.* .

DALEY, R. 1991 *Atmospheric Data Analysis*. Cambridge University Press.

FOIAS, C. & TEMAM, R. 1984 Determination of the solutions of the Navier-Stokes equations by a set of nodal values. *Math. Comput.* **43**, 117–133.

FOIAS, C. & TITI, E. 1984 Determining nodes, finite difference schemes and inertial manifolds. *Nonlinearity* **4**, 135–153.

HALLBÄCK, M. 1993 Development and critical evaluation of turbulent models through direct numerical simulation of homogeneous turbulence. *Tech. Rep.* 1993:2. Department of Mechanics, Royal Institute of Technology.

HENSHAW, W. & KREISS, H.-O. 1991 A numerical study of the propagation of perturbations in the solutions of the 2D incompressible Navier-Stokes equations. In *Third International Conference on Hyperbolic Problems* (ed. B. Engquist & B. Gustafsson), pp. 54–61. Chartwell-Bratt.

HENSHAW, W., KREISS, H.-O. & REYNA, L. 1989 On the smallest scale for the incompressible Navier-Stokes equations. *Theoretical and Computational Fluid Dynamics* **1**, 1–32.

HENSHAW, W., KREISS, H.-O. & REYNA, L. 1990 Smallest scale estimates for the incompressible Navier-Stokes equations. *Arch. Rational Mech. Anal.* **112**, 21–44.

HENSHAW, W., KREISS, H.-O. & YSTRÖM, J. 2001 Numerical experiments on the interaction between the large- and small-scale motion of the Navier-Stokes equations. Research Report This report. Lawrence Livermore National Laboratory.

JONES & TITI, S. 1993 Upper bounds on the number of determining modes, nodes, and volume elements for the Navier-Stokes equations. *Indiana Univ. Math. J.* **42**, 875–887.

KREISS, H. & YSTRÖM, J. 1998 A numerical study of the solution to the 3d incompressible Navier-Stokes equations. *Tech. Rep.* 98-24. Dep. of Math. University of California.

LESIUER, M. 1990 *Turbulence in Fluids*. Boston: Kluwer Academic Publishers.

LUNDBLADH, A., HENNINGSON, D. & JOHANSSON, A. 1992 An efficient spectral integration method for the solution of the Navier-Stokes equations. *Tech. Rep.* FFA-TN 1992-28. The Aeronautical Research Institute of Sweden.

MCWILLIAMS, J. C. 1984 The emergence of isolated coherent vorticies in turbulent flow. *Journal of Fluid Mechanics* **146**, 21–43.

ORSZAG, S. A. 1970 Analytical theories of turbulence. *Journal of Fluid Mechanics* **41** (2), 363–386.

SAFFMAN, P. 1992 *Vortex Dynamics*. Cambridge: Cambridge University Press.

TALAGRAND, O. 1981 A study of the dynamics of four dimensional data assimilation. *Tellus* **33**, 43–60.

TATSUMI, T. 1980 Theory of homogeneous turbulence. *Advances in Applied Mechanics* **20** (39–133).

THOMPSON, P. 1969 Reduction of analysis error through constraints of dynamical consistency. *Journal of Applied Meteorology* **8**, 739–742.

WHITHAM, G. 1974 *Linear and Nonlinear Waves*. John Wiley and Sons, New York.

WILLIAMSON, D. & DICKINSON, R. 1972 Periodic updating of meteorological variables. *Journal of Atmospheric Science* **29**, 191–193.